ESAIM: M2AN 52 (2018) 1501–1532
https://doi.org/10.1051/m2an/2017006

**ESAIM: Mathematical Modelling and Numerical Analysis**
www.esaim-m2an.org

# AN ADJOINT-BASED METHOD FOR THE NUMERICAL APPROXIMATION OF SHAPE OPTIMIZATION PROBLEMS IN PRESENCE OF FLUID-STRUCTURE INTERACTION

Andrea Manzoni[1,*] and Luca Ponti[2]

**Abstract.** In this work, we propose both a theoretical framework and a numerical method to tackle shape optimization problems related with fluid dynamics applications in presence of fluid-structure interactions. We present a general framework relying on the solution to a suitable adjoint problem and the characterization of the shape gradient of the cost functional to be minimized. We show how to derive a system of (first-order) optimality conditions combining several tools from shape analysis and how to exploit them in order to set a numerical iterative procedure to approximate the optimal solution. We also show how to deal efficiently with shape deformations (resulting from both the fluid-structure interaction and the optimization process). As benchmark case, we consider an unsteady Stokes flow in an elastic channel with compliant walls, whose motion under the effect of the flow is described through a linear Koiter shell model. Potential applications are related *e.g.* to design of cardiovascular prostheses in physiological flows or design of components in aerodynamics.

**Mathematics Subject Classification.** 49Q10, 49J20, 65K10, 65N30, 74F10, 76D55.

Received May 31, 2016. Accepted February 24, 2017.

## 1. Introduction

The efficient numerical solution to PDE-constrained optimization problems is of key importance in many contexts of applied sciences and engineering. Relevant instances within this broad class of problems are *e.g.* heat/flow control, reduction of plant emissions, design of wing profiles for the sake of efficiency, flow laminarization, and many others [23, 24, 29, 30]. In all these cases, a state system described in terms of partial differential equations (PDEs) has to be controlled in order to reach a physically meaningful target, by acting *e.g.* on distributed/boundary controls, PDE coefficients, or the shape of the domain itself. The target is usually expressed in terms of minimization of a suitable cost functional, depending on the solution to the state problem – in this sense the state system plays the role of a constraint – in addition to control variables.

In this paper, we focus on shape optimization problems, where the shape of the domain $\Omega$ on which the state system is defined plays the role of control variable. In abstract form, a shape optimization problem can be

*Keywords and phrases.* PDE-constrained optimization, shape optimization, fluid-structure interaction, adjoint problem.

[1] CMCS-MATHICSE-SB, Ecole Polytechnique Fédérale de Lausanne, Station 8, 1015 Lausanne, Switzerland.

[2] Dipartimento di Matematica "F. Brioschi", Politecnico di Milano, *via* Bonardi 9, 20133 Milano, Italy.

*Corresponding author: andrea.manzoni@epfl.ch

formulated as the minimization, over a set of admissible shapes $\mathcal{O}_{ad}$, of a cost functional $J(\Omega) = \tilde{J}(\Omega, y(\Omega))$; in our case, this latter also depends on the *state variable* $y(\Omega) \in V$, which solves a – possibly, nonlinear and time-dependent – PDE, that is:

$$J(\hat{\Omega}) = \min_{\Omega \in \mathcal{O}_{ad}} J(\Omega) \qquad \text{s.t.} \qquad E(\Omega, y(\Omega; t)) = 0 \quad \text{in} \quad V'.$$

For the case at hand, $J : \mathcal{O}_{ad} \to \mathbb{R}$ is a cost functional evaluated over $(0, T)$, $\mathcal{O}_{ad}$ is a set of domains which fulfill some (problem-dependent, physically meaningful) constaints, $V$ is a suitable functional space (defined over $\Omega$, and depending on time $t \in (0, T)$) and $V'$ its dual; the equation $E(\Omega, y(\Omega; t)) = 0$ in $V'$ represents the (abstract) formulation of the time-dependent *state problem*.

In particular, we address the case of shape optimization problems arising in fluid mechanics, because of their relevance in many applied contexts, such as aerospace, naval and biomedical engineering [8, 14]. In all these cases, a very general problem is represented by the optimal design of aerodynamic/hydrodynamic structures in order to minimize *e.g.* the energy dissipation of the fluid, or resistance forces, or fluid vorticity and stresses, or again the compliance of the structure itself (and then maximize its deformation resistance). Nevertheless, in many problems of real-life interest, the goal is to optimize the shape of a flexible structure within a fluid flow, for which fluid-structure interaction (FSI) phenomena cannot be neglected. In fact, the interaction of such a structure with the fluid – such as in the case *e.g.* of blood flows through arteries and compliant vessels [11, 12], aeroelastic instabilities in aircrafts [17], turbomachinery design [34] – yield several physical phenomena which may have a strong impact on the solution to the optimal design problem, too.

FSI problems usually involve a physical system made by a fluid component (*e.g.* air, water or blood) close to a solid structural component (such as a wing or a vessel). The interaction between the fluid and the structure leads to a structural displacement, followed by a deformation of the domains in which both the fluid and the solid components are defined, thus making the domain of the system an unknown itself. Solving an optimal design problem in this context thus features additional difficulties, because of the need to consider shape deformations due to either FSI effects and the optimization pipeline. A possible way to partially overcome this difficulty is to rely on a *fixed domain* approach, in which the state FSI problem is rewritten on a fixed reference domain (see *e.g.* [36,37,43]), whose shape is the object of the optimization. Tackling a shape optimization problem in presence of FSI is thus a huge computational challenge, for which very few results are currently available in literature. Moubachir and Zolésio present a theoretical analysis of optimal flow control problems (not a shape optimization problem, though) involving FSI in [38], where the goal is to minimize the displacement of a compliant wall pipe in which the fluid is flowing using the inlet velocity as control variable. From a computational point of view, some ideas related with iterative algorithms for the solution to shape optimization problems in presence of FSI are addressed in [26, 48], but relying on a *black-box* approach and without deriving explicitly a system of optimality conditions involving the shape gradient of the cost functional. A recent application of shape optimization tools to the numerical solution to free-boundary problems has been proposed in [15].

The main goal of this paper is to present some analytical and numerical methods for the solution to shape optimization problems when dealing with applications involving FSI effects. We pursue an *optimize-then-discretize* approach [7, 27, 40, 45]: first, we derive the optimality conditions related with the PDE-constrained optimization problem, relying on the Lagrange multiplier approach, and showing how to handle shape variations and derivatives. To simplify the system of (first order, necessary) optimality condition we introduce a suitable *adjoint problem*, whose derivation is not as straightforward as, *e.g.*, in the case of fluid flows in presence of rigid walls/bodies. Then we set up an efficient numerical algorithm to approximate the solution to the shape optimization problem, combining (i) a *partitioned* FSI solver; (ii) a descent method for numerical optimization; (iii) a Free Form Deformation (FFD) map to efficiently describe shape deformations at each iteration of the optimization problem. The application which inspires the analysis reported in this work is the optimal design of a bypass graft to restore blood perfusion downfield an occluded coronary artery. A common goal may be, *e.g.*, to minimize the flow vorticity in proximity of the junction between the graft and the host occluded artery. Many works (see, *e.g.*, [32, 33, 36] and references therein) have focused on such a problem, typically by acting on the

wall shape near the anastomosis by local shape variations. Nevertheless, FSI effects have never been considered when dealing with this application.

In this work we consider an idealized two-dimensional viscous Newtonian flow at low Reynolds numbers (modelled by unsteady Stokes equations) in an elastic domain described by means of a mono-dimensional *linear Koiter shell model*. This model [10, 19, 39, 41] is based on the assumption that the structure is *thin* (compared to the fluid domain) and can be deformed, as a consequence of the interaction between fluid and solid, mainly in the normal direction to the surface. To deal with the domain motion and formulate the fluid problem we rely on the so-called *arbitrary Lagrangian-Eulerian* (ALE) formalism, following a common approach in the FSI framework (see, *e.g.*, [19]). Although we consider a *prototypical example* on a simple rectangular domain in undeformed configuration, the derivation of the system of optimality conditions, are of general interest and can be applied to any optimal design problem including the features above. The presented setting can be considered as a first step towards performing shape optimization with a moving domain, considering for the time being the case of a linear Stokes flow and a simple shell model for the structure, in order to highlight the difficulties related with (i) FSI terms and (ii) shape derivatives, although the proposed framework could be also extended to the case of Navier-Stokes equations; see, *e.g.*, [35] for further details on the formulation of a FSI problem including three-dimensional Navier-Stokes flows interacting with a structure represented by a two-dimensional quasilinear elastic model of Koiter shell type. Indeed, the Navier-Stokes case would fit even better the ALE formulation, with the ALE velocity incorporated in the convective term. In such a case, as well as when considering more general structural models, the procedure to derive a set of optimality conditions presented in the paper could be also exploited, however featuring more terms to deal with due to the nonlinearity of the flow model and the possibly more complex structure equation. From the computational standpoint, to deform the domain, we implement a Free-Form Deformation (FFD) map based on non rational uniform B-splines (NURBS) [31, 46, 47]; this option enables to exploit the low dimensionality of the classic FFD map combined with the flexibility on the choice of the degrees of freedom, typical of NURBS representations.

The structure of the paper is as follows. We introduce a two dimensional FSI problem in Section 2 alongside the abstract formulation of the shape optimization to analyze. In Section 3 we derive a system of first order optimality conditions exploiting the Lagrange multipliers method; in particular, classical differentiation and shape differentiation results are employed in order to obtain the adjoint problem for the structural subproblem. In Section 4 we describe a partitioned iterative scheme to solve the state FSI problem based on a Dirichlet−Neumann approach [9, 41]; then, we show how to suitably modify this procedure in order to solve the (time backward) adjoint FSI problem. Moreover, we introduce a steepest descent-like procedure based on the gradient method, in order to solve the shape optimization problem numerically. Numerical results obtained through the proposed framework are shown in Section 5, in order to assess both the theoretical results provided in the paper and the computational performances of the proposed algorithm. We also report a comparison with the solution to the same problem in a rigid geometry, for which existing results are available in literature.

## 2. Definition of the problem

We consider the flow of an unsteady incompressible viscous fluid in a domain $\Omega(t) \subset \mathbb{R}^2$, $t \in [0, T)$. The boundary portion $\Gamma(t) \subset \partial\Omega(t)$ is bounded by a thin deformable wall modeled by means of the Koiter model; for this reason, the shape of the interface $\Gamma(t)$ and of the domain $\Omega(t)$ are unknown and depend on the interaction between the fluid and the structure itself. Moreover, we suppose that the portion $\partial\Omega(t) \setminus \Gamma(t)$ is rigid, thus fixed in time. We also assume that structural displacements $\boldsymbol{\eta}$ are allowed only in vertical direction, that is, $\boldsymbol{\eta} = (0, \eta)^T$. We also introduce a one-dimensional reference domain

$$\Gamma_0 = \{(x_1, x_2) : x_1 \in (0, L), x_2 = x_{2,0}\},$$

so that

$$\Gamma(t) = \{(x_1, x_2) : x_1 \in (0, L), x_2 = x_{2,0} + \eta(x_1, t)\} = (I + \eta\, \mathbf{e}_2) \circ \Gamma_0, \qquad t > 0, \tag{2.1}$$

where $\{\mathbf{e}_i\}_{i=1,2}$ denote the unit vectors of the canonical basis of $\mathbb{R}^2$ and $x_{2,0} \in \mathbb{R}$ a given constant. For the sake of notation, we set $\Gamma(0) \equiv \Gamma_0$; in the same way, we denote by $\Omega(0) \equiv \Omega_0$ the fluid domain at $t = 0$.

Thus, given a forcing term $f(t) \in L^2(\Gamma_0)$ for all $t \in (0,T)$, the structural displacement $\eta = \eta(\cdot,t)$ is given by the solution to the following one-dimensional structural problem [19,39,41]:

$$\begin{cases} \rho_S h_S \dfrac{\partial^2 \eta}{\partial t^2} - \mu_S \dfrac{\partial^2 \eta}{\partial x_1^2} + \beta\eta = f(t) & \text{in} \quad \Gamma_0 \times (0,T) \\ \eta(0,t) = \eta(L,t) = 0 & t \in (0,T) \\ \eta(x_1,0) = \dfrac{\partial \eta}{\partial t}(x_1,0) = 0 & \mathbf{x} \in \Gamma_0 \end{cases} \tag{2.2}$$

being $\rho_S > 0$, $\mu_S > 0$ and $h_S > 0$ the density, the viscosity and the thickness of the solid structure, respectively; the coefficient $\beta > 0$ depends on the physical and geometrical properties of the structure, too (see *e.g.* [41]). Note that, for the sake of the structural problem definition, we identify $\Gamma_0 \subset \mathbb{R}^2$ with interval $\Gamma_0 = (0,L) \subset \mathbb{R}$ since the second coordinate $x_2$ is constant and equal to $x_{2,0}$ and the structure displacements only occur in the vertical direction. For this reason, hereon we treat the structural problem as a one-dimensional problem, by considering $\Gamma(t)$ as the set of points defining the nonrigid boundary of the fluid domain.

To describe the fluid flow, we consider the unsteady Stokes equations for an incompressible Newtonian fluid. For the sake of simplicity, we focus on low Reynolds number flows ($Re \ll 1$), for which nonlinear advective terms are neglected; nevertheless, extending the proposed framework for shape optimization the case of Navier-Stokes equations (moderate Reynolds number flows) does not features extreme difficulties concerning both the derivation of optimality conditions and the setting of a numerical approximation scheme.

To deal with the deformations of the fluid domain, we formulate Stokes equations following the so-called ALE formalism; for this reason, we introduce a reference computational domain $\tilde{\Omega}$ and the so-called ALE map

$$\tilde{\mathcal{A}} : \tilde{\Omega} \times \mathbb{R}^+ \to \mathbb{R}^2, \qquad \mathbf{x} = \tilde{\mathcal{A}}(\tilde{\mathbf{x}}, t), \tag{2.3}$$

which maps each point $\tilde{\mathbf{x}} \in \tilde{\Omega}$ into the corresponding point $\mathbf{x}$ of the current configuration $\Omega(t)$, for any $t > 0$. Furthermore, we denote by $\tilde{\mathcal{A}}_t(\cdot) = \tilde{\mathcal{A}}(\cdot,t)$ and by $Q_T = \{(\mathbf{x},t) \in \mathbb{R}^2 \times (0,T) \text{ such that } \mathbf{x} \in \Omega(t)\}$ the space-temporal cylinder where the fluid problem is defined. Then, for any function $q$ taking values in $Q_T$, we define its ALE time derivative [42] as

$$\left.\frac{\partial q}{\partial t}\right|_{\tilde{\mathcal{A}}} := \frac{\mathrm{d}}{\mathrm{d}\,t} q(\tilde{\mathcal{A}}_t(\tilde{\mathbf{x}}), t) = \frac{\partial q}{\partial t} + \mathbf{w} \cdot \nabla q \tag{2.4}$$

where $\mathbf{w} : \Omega(t) \times (0,T) \to \mathbb{R}^2$ is the velocity of the domain deformed *via* the ALE map (or domain deformation velocity),

$$\mathbf{w}(\cdot,t) = \frac{\partial \tilde{\mathcal{A}}_t}{\partial t} \circ \tilde{\mathcal{A}}_t^{-1}, \qquad t \geq 0. \tag{2.5}$$

and $\frac{\partial q}{\partial t}$ denotes the *standard* Eulerian time derivative.

For the case at hand, the deformation of the domain is caused by the vertical displacement of the solid structure on the boundary $\Gamma(t)$, as shown in (2.1). Hence, the ALE map has to fulfill

$$\tilde{\mathcal{A}}_t(\mathbf{x}_0) = \mathbf{x}_0 + \eta(x_1,t)\mathbf{e}_2 \qquad \forall \mathbf{x}_0 \in \Gamma_0.$$

To define the ALE map at time $t$, we do an harmonic extension of $\mathbf{x}_0 + \eta(x_1,t)\mathbf{e}_2$ onto the whole domain $\Omega_0$, that is,

$$\tilde{\mathcal{A}}_t(\mathbf{x}_0) = \mathbf{d} \qquad \text{where} \qquad \mathbf{d} \text{ solves} \begin{cases} -\Delta \mathbf{d} = \mathbf{0} & \text{in} \quad \Omega_0 \\ \mathbf{d} = \mathbf{0} & \text{on} \quad \partial\Omega_0 \setminus \Gamma_0 \\ \mathbf{d} = \mathbf{x}_0 + \eta(x_1,t)\mathbf{e}_2 & \text{on} \quad \Gamma_0. \end{cases} \tag{2.6}$$

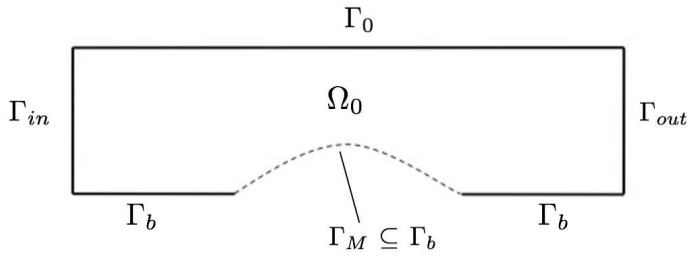


FIGURE 1. Reference domain configuration (used as starting point for optimization in test cases 1, 2 and 3).

We opt for this construction since we need to know the ALE mapping (and the corresponding domain deformation velocity) only at discrete time levels, where the approximation of the problem is sought (see Sect. 4); see, *e.g.*, [20] for further details and alternative approaches.

The Stokes equations in the ALE reference coordinates read as follows:

$$\begin{cases} \rho_F \left.\dfrac{\partial \mathbf{u}}{\partial t}\right|_{\tilde{\mathcal{A}}} - \rho_F \mathbf{w}\cdot\nabla\mathbf{u} + \nabla p - \mu_F \Delta\mathbf{u} = 0 & \text{in} \quad Q_T \\ \nabla\cdot\mathbf{u} = 0 & \text{in} \quad Q_T \\ \mathbf{u} = \mathbf{u}_{\text{in}} & \text{on} \quad \Gamma_{\text{in}}\times(0,T) \\ -p\,\mathbf{n} + \nu\dfrac{\partial \mathbf{u}}{\partial \mathbf{n}} = 0 & \text{on} \quad \Gamma_{\text{out}}\times(0,T) \\ \mathbf{u} = 0 & \text{on} \quad \Gamma_b\times(0,T) \\ \mathbf{u}|_{t=0} = \mathbf{u}_0 & \text{in} \quad \Omega_0 \end{cases} \tag{2.7}$$

being $\mathbf{u} = \mathbf{u}(\mathbf{x},t)$ the fluid velocity and $p = p(\mathbf{x},t)$ the fluid pressure, respectively. Moreover, $\Gamma_{\text{in}}$ denotes the inlet boundary, $\Gamma_{\text{out}}$ the outlet boundary and $\Gamma_b$ the boundary portion on which we impose homogeneous Dirichlet conditions – expressing, *e.g.*, a no-slip condition between the fluid and a rigid structure, see Figure 1. Note that $\partial\Omega(t) = \Gamma_{\text{in}} \cup \Gamma_{\text{out}} \cup \Gamma_b \cup \Gamma(t)$. In order to couple the structure problem (2.2) and the fluid problem (2.7), we prescribe some conditions at the interface $\Gamma(t)$. In particular, we impose the continuity of the velocity and of the normal stress at the interface, for any $t \in [0,T)$, as follows:

$$\begin{cases} \mathbf{u}|_{\Gamma(t)} = \left.\left(\dfrac{\partial\eta}{\partial t}\circ\tilde{\mathcal{A}}_t^{-1}\right)\right|_{\Gamma(t)} \mathbf{e}_2\,, \\ f = -\,\mathcal{J}\,\left(\boldsymbol{\sigma}^F(\mathbf{u},p)\,\mathbf{n}\right)\big|_{\Gamma(t)}\cdot\mathbf{e}_2\,; \end{cases} \tag{2.8}$$

$\mathbf{n}$ is the unit outward normal on $\Gamma(t)$, $\boldsymbol{\sigma}^F(\mathbf{u},p) = \mu_F(\nabla\mathbf{u}+\nabla^T\mathbf{u}) - pI$ is the Cauchy stress tensor related to the fluid and $\mathcal{J} = \sqrt{1+(\partial\eta/\partial x_1)^2}$ is the Jacobian of the transformation from Eulerian to Lagrangian coordinates. Note that, by comparing (2.5) and $(2.8)_1$, we obtain the following identity:

$$\mathbf{w} = (\mathbf{u}\cdot\mathbf{e}_2)\mathbf{e}_2 \qquad \text{on} \qquad \Gamma(t). \tag{2.9}$$

We are now ready to formulate our shape optimization problem. Our goal is to determine the best shape $\hat{\Omega}$ of the domain $\Omega_0$ over a set of admissible shapes $\mathcal{O}_{ad}$, such that the energy dissipated by the fluid is minimized. To this aim, we assume that we can only *optimize* a portion $\Gamma_M \subseteq \Gamma_b$ of the portion $\Gamma_b \subset \partial\Omega_0$ of the boundary

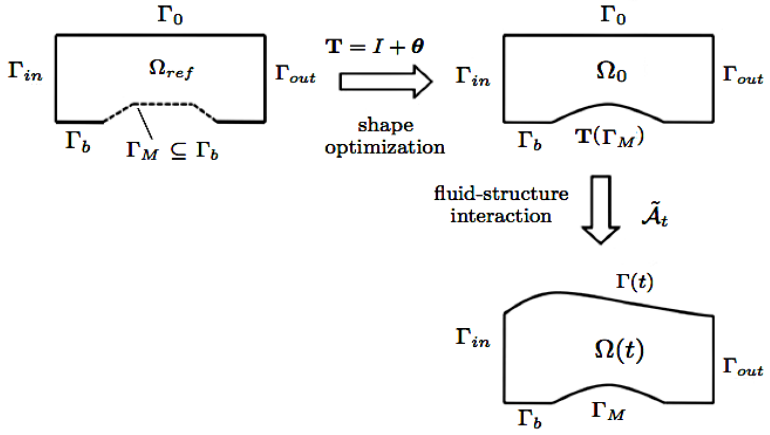


FIGURE 2. Graphical sketch of the interplay between shape optimization and the fluid-structure interaction. Admissible shapes for $\Omega_0$ are obtained from the reference domain $\Omega_{\text{ref}}$ performing deformations under the form $I + \boldsymbol{\theta}$; during the solution of the state FSI problem, the domain $\Omega_0$ undergoes geometrical deformations yielding the evolution $\{\Omega(t),\, t \in [0,T)\}$.

(related to the bottom part in Fig. 2); we point out that the shape of this boundary portion is rigid, therefore it can only be deformed during the shape optimization process.

In abstract form, we can write the shape optimization problem as follows: find $\hat{\Omega} \in \mathcal{O}_{ad}$ so that

$$J(\hat{\Omega}) = \min_{\Omega \in \mathcal{O}_{ad}} J(\Omega), \tag{2.10}$$

where the cost functional $J(\Omega) = \tilde{J}(\Omega, \mathbf{u}(\Omega))$ is given by

$$\tilde{J}(\Omega, \mathbf{u}(\Omega)) = \frac{\alpha}{2} \int_0^T \int_{\Omega(t)} |\nabla \mathbf{u}(\Omega(t))|^2 \, \mathrm{d}\mathbf{x} \, \mathrm{d}t, \tag{2.11}$$

$(\mathbf{u}, p, \eta) = (\mathbf{u}(\Omega), p(\Omega), \eta(\Omega))$ solve the state FSI problem (2.2), (2.7), (2.8), and the set of admissible shapes $\mathcal{O}_{ad}$ is

$$\mathcal{O}_{ad} = \{\Omega \in \mathcal{O} :\ \Gamma_{\text{in}} \cup \Gamma_{\text{out}} \cup \Gamma_0 \cup \Gamma_b \setminus \Gamma_M \subset \partial\Omega \text{ is fixed and } |\Omega| = V_0\} \subset \mathcal{O}, \tag{2.12}$$

where $V_0 > 0$ is a prescribed volume. Following a common approach in shape optimization, we introduce a (bounded, Lipschitz) reference domain $\Omega_{\text{ref}}$, and we define the admissible shapes as the images of $\Omega_{\text{ref}}$ through the application of a *perturbation of identity* map. Thus, each admissible shape $\Omega \in \mathcal{O}$ can be written as

$$\Omega = \{\mathbf{x} \in \mathbb{R}^2 : \mathbf{x} = \mathbf{T}(\mathbf{x}_{\text{ref}}),\ \mathbf{x}_{\text{ref}} \in \Omega_{\text{ref}}\} \quad \text{with} \quad \mathbf{T}(\mathbf{x}_{\text{ref}}) = \mathbf{x}_{\text{ref}} + \boldsymbol{\theta}(\mathbf{x}_{\text{ref}}), \tag{2.13}$$

where $\boldsymbol{\theta} \in W^{1,\infty}(\Omega_{\text{ref}}; \mathbb{R}^2)$ is a vector field such that $\|\boldsymbol{\theta}\|_{W^{1,\infty}} \leq 1$; here $W^{k,p}(\Omega_{\text{ref}}; \mathbb{R}^d) = \{\mathbf{v} \in (L^p(\Omega_{\text{ref}}))^d :\ D_\alpha u_i \in L^p(\Omega_{\text{ref}})\ \forall i \in \{1, \ldots, d\},\ \forall |\alpha| \leq k\}$, with $1 \leq p \leq +\infty$, and the usual multi-index notation is used. This property ensures that the map $\mathbf{T} = I + \boldsymbol{\theta}$ induces small deformations, and is a diffeomorphism (see *e.g.* [1], Lem. 6.13). For the case at hand, this property also ensures that contact with the top part $\Gamma_0$ of the boundary is avoided. Figure 2 shows the relationship between the different kinds of domain introduced so far. In particular, the map $\mathbf{T} = I + \boldsymbol{\theta}$ transforms the reference domain $\Omega_{\text{ref}}$ into the admissible shapes $\Omega_0$, among which $\hat{\Omega}$ is the optimal one. Recall that the domains $\Omega(t)$ are defined as a deformation of the initial domain $\Omega_0$, as a consequence of the interaction between the structure and the fluid flow. The optimal shape is thus obtained by iteratively deforming the reference domain, until a suitable optimality criterion is fulfilled.

Ensuring the well-posedness of the shape optimization problem, in and of itself a hard task from a theoretical standpoint, is even more complicated in the case at hand, because there is no theoretical result which asserts that the FSI state problem (2.2)–(2.8) admits a weak solution. Note that the situation would be different in the Navier-Stokes case for which the presence of the advection term – although featuring further difficulties because of its nonlinear nature – allows to state global-in-time existence of solutions by establishing suitable energy inequalities.

## 3. Optimality conditions

In this section we show how to derive a system of (first-order, necessary) optimality conditions exploiting the Lagrange multipliers method, in the case of a shape optimization problem where the state variables are solutions of a FSI problem. For a general introduction to the Lagrange multipliers method in optimal control problems see, *e.g.*, [23, 28]; a detailed characterization to the case of optimal design problems can be found in [1, 13]. The general idea is to rewrite the problem under the form of a PDE-constrained optimization problem, and to characterize its solution as the saddle points of a Lagrangian functional $\mathcal{L}$. This latter is obtained by introducing a set of Lagrange multipliers to take into account the cost functional with the constraints given by the state equation under weak form, and related boundary and initial conditions. In order to define the Lagrangian functional, let us introduce the following time-dependent functional spaces [38]:

$$X_F^t(\Omega) = \{\mathbf{v} \in H^1_{\Gamma_b}(\Omega(t);\mathbb{R}^2) : \mathbf{v}|_{\Gamma_{\rm in}} = \mathbf{u}_{\rm in}\},$$

$$V_F(\Omega) = H^1(0,T;(H^2(\Omega(t));\mathbb{R}^2) \cap X_F^t), \qquad V_0(\Omega) = H^1(0,T;(H^2(\Omega(t));\mathbb{R}^2) \cap H^1_{\Gamma_{\rm in}\cup\Gamma_b}(\Omega(t);\mathbb{R}^2)),$$

$$Q_F(\Omega) = H^1(0,T;H^1(\Omega(t))), \qquad V_S = H^2(0,T;H^2(\Gamma_0) \cap H^1_{\{0\}\cup\{L\}}(\Gamma_0)).$$

To couple the weak formulation of the fluid problem and the structure model, we introduce the following functional space which yields the continuity of the velocity through the interface $\Gamma(t)$:

$$S(\Omega) = \{(\mathbf{v},\psi) \in V_0(\Omega) \times V_S \text{ s.t. } \mathbf{v}(t)|_{\Gamma(t)} = (\psi \circ \tilde{\mathcal{A}}_t^{-1})\mathbf{e}_2 \quad \forall t \in (0,T)\}.$$

Furthermore, let us denote by $(\mathbf{v},\psi,q) \in S(\Omega) \times Q_F(\Omega)$ the Lagrangian multipliers (or *adjoint variables*) corresponding to the state variables. Hence, we can define the following Lagrangian functional:

$$\begin{aligned}
\mathcal{L}(\mathbf{u},p,\eta\,;\,\mathbf{v},q,\psi\,;\boldsymbol{\lambda}_F,&\lambda_S,\lambda_S^0,\lambda_S^1;\,\Omega) = \frac{\alpha}{2}\int_0^T \int_{\Omega(t)} |\nabla \mathbf{u}|^2 \mathrm{d}\mathbf{x}\,\mathrm{d}t \\
&- \int_0^T \int_0^L \left(\rho_S h_S \frac{\partial^2 \eta}{\partial t^2}\psi + \mu_S \frac{\partial \eta}{\partial x_1}\frac{\partial \psi}{\partial x_1} + \beta\eta\psi\right) \mathrm{d}x_1\,\mathrm{d}t \\
&- \int_0^T \int_{\Omega(t)} \left(\rho_F \frac{\partial \mathbf{u}}{\partial t}\cdot\mathbf{v} - p\,\nabla\cdot\mathbf{v} + \mu_F \nabla\mathbf{u} : \nabla\mathbf{v} - q\,\nabla\cdot\mathbf{u}\right) \mathrm{d}\mathbf{x}\,\mathrm{d}t \\
&+ \int_0^T \int_{\Gamma_D} \boldsymbol{\lambda}_F \cdot (\mathbf{u} - \mathbf{u_D})\,\mathrm{d}\sigma\,\mathrm{d}t + \int_0^T [\lambda_S \eta]_0^L\,\mathrm{d}t + \int_0^L \left(\lambda_S^0\,\eta(0) + \lambda_S^1 \frac{\partial \eta}{\partial t}(0)\right) \mathrm{d}x_1, \quad (3.1)
\end{aligned}$$

where the Dirichlet boundary conditions and the initial conditions, defined in the state problem, are introduced by means of the Lagrangian multipliers $\boldsymbol{\lambda}_F \in L^2(0,T;H^1(\mathbb{R}^2))$, $\lambda_S \in L^2(0,T)$, $\lambda_S^0 \in L^2(\Gamma_D)$ e $\lambda_S^1 \in L^2(\Gamma_D)$ (for further details on this latter point, see *e.g.* [1, 3]). Here we have set

$$\Gamma_D = \Gamma_b \cup \Gamma_{\rm in} \qquad \text{and} \qquad \mathbf{u}_D = \begin{cases} \mathbf{0} & \text{on} \quad \Gamma_b \\ \mathbf{u}_{\rm in} & \text{on} \quad \Gamma_{\rm in}. \end{cases}$$

In order to simplify the derivation of the optimality condition, it is convenient to integrate by parts the term $\int_0^T \int_{\Omega(t)} (\rho_F \frac{\partial \mathbf{u}}{\partial t}\cdot\mathbf{v})\,\mathrm{d}\mathbf{x}\,\mathrm{d}t$ appearing in (3.1). By using the Reynolds transport theorem to deal with the derivation

of the integral defined over the time-dependent domain $\Omega(t)$ (see *e.g.* [16]), we obtain the following identity:

$$\int_0^T \int_{\Omega(t)} \frac{\partial \mathbf{u}}{\partial t} \cdot \mathbf{v} \, \mathrm{d}\mathbf{x} \, \mathrm{d}t = - \int_0^T \int_{\Omega(t)} \mathbf{u} \cdot \frac{\partial \mathbf{v}}{\partial t} \, \mathrm{d}\mathbf{x} \, \mathrm{d}t - \int_0^T \int_{\Gamma(t)} (\mathbf{u} \cdot \mathbf{v})(\mathbf{u}_S \cdot \mathbf{n}) \mathrm{d}\sigma \mathrm{d}t + \int_{\Omega(T)} \mathbf{u}(T) \cdot \mathbf{v}(T) \, \mathrm{d}\mathbf{x} \, \mathrm{d}t - \int_{\Omega_0} \mathbf{u}_0 \cdot \mathbf{v}(0) \, \mathrm{d}\mathbf{x} \, \mathrm{d}t \,, \quad (3.2)$$

where $\mathbf{u}_S = (\frac{\partial \eta}{\partial t} \circ \eta^{-1}) \, \mathbf{e}_2$ is the velocity of the interface $\Gamma(t)$. Thus, the Lagrangian functional $\mathcal{L}$ can be equivalently rewritten as follows:

$$\begin{aligned}
\mathcal{L}(\mathbf{u}, p, \eta \,; \mathbf{v}, q, \psi \,; \boldsymbol{\lambda}_F, \lambda_S, \lambda_S^0, \lambda_S^1; \, \Omega) = {} & \frac{\alpha}{2} \int_0^T \int_{\Omega(t)} |\nabla \mathbf{u}|^2 \, \mathrm{d}\mathbf{x} \, \mathrm{d}t \\
& - \int_0^T \int_0^L \left( \rho_S h_S \frac{\partial^2 \eta}{\partial t^2} \psi + \mu_S \frac{\partial \eta}{\partial x_1} \frac{\partial \psi}{\partial x_1} + \beta \eta \psi \right) \mathrm{d}x_1 \, \mathrm{d}t \\
& - \int_0^T \int_{\Omega(t)} \left( -\rho_F \mathbf{u} \cdot \frac{\partial \mathbf{v}}{\partial t} - p \, \nabla \cdot \mathbf{v} + \mu_F \nabla \mathbf{u} : \nabla \mathbf{v} - q \, \nabla \cdot \mathbf{u} \right) \mathrm{d}\mathbf{x} \, \mathrm{d}t \\
& + \int_0^T \int_{\Gamma_D} \boldsymbol{\lambda}_F \cdot (\mathbf{u} - \mathbf{u_D}) \, \mathrm{d}\sigma \, \mathrm{d}t + \rho_F \int_0^T \int_{\Gamma(t)} (\mathbf{u} \cdot \mathbf{v})(\mathbf{u}_S \cdot \mathbf{n}) \, \mathrm{d}\sigma \, \mathrm{d}t - \rho_F \int_{\Omega(T)} \mathbf{u}(T) \cdot \mathbf{v}(T) \, \mathrm{d}\mathbf{x} \\
& + \rho_F \int_{\Omega_0} \mathbf{u}_0 \cdot \mathbf{v}(0) \, \mathrm{d}\mathbf{x} + \int_0^T [\lambda_S \eta]_0^L \, \mathrm{d}t \\
& + \int_0^L \left( \lambda_S^0 \, \eta(0) + \lambda_S^1 \, \frac{\partial \eta}{\partial t}(0) \right) \mathrm{d}x_1. \qquad (3.3)
\end{aligned}$$

By deriving the Lagrangian functional (3.3) with respect to the adjoint variables $(\mathbf{v}, \psi, q)$ and imposing that these derivatives vanish, we obtain the weak formulation of the state problem (2.2)–(2.8). By deriving $\mathcal{L}$ with respect to the state variables, we recover the expression of the adjoint problem. Far from being a trivial task for the case at hand, we show how to obtain the expression of the adjoint problem in the following subsections.

### 3.1. Fluid adjoint problem

We now characterize the fluid adjoint problem. By deriving the Lagrangian with respect to the fluid variables $(\mathbf{u}, p)$ and requiring that the resulting derivatives vanish for every variation $(\delta\mathbf{u}, \delta p) \in V_F(\Omega) \times Q_F(\Omega)$, we obtain

$$\left\langle \frac{\partial \mathcal{L}}{\partial p}, \delta p \right\rangle = \int_0^T \int_{\Omega(t)} \delta p \, \nabla \cdot \mathbf{v} \, \mathrm{d}\mathbf{x} \, \mathrm{d}t = 0 \qquad \forall \delta p \in Q_F(\Omega),$$

$$\begin{aligned}
\left\langle \frac{\partial \mathcal{L}}{\partial \mathbf{u}}, \delta \mathbf{u} \right\rangle = {} & - \alpha \int_0^T \int_{\Omega(t)} \Delta \mathbf{u} \cdot \delta \mathbf{u} \, \mathrm{d}\mathbf{x} \, \mathrm{d}t + \alpha \int_0^T \int_{\partial\Omega(t)} \frac{\partial \mathbf{u}}{\partial \mathbf{n}} \cdot \delta \mathbf{u} \, \mathrm{d}\sigma \, \mathrm{d}t \\
& - \int_0^T \int_{\Omega(t)} \left( -\rho_F \delta \mathbf{u} \cdot \frac{\partial \mathbf{v}}{\partial t} - \mu_F \delta \mathbf{u} \cdot \Delta \mathbf{v} + \nabla q \cdot \delta \mathbf{u} \right) \mathrm{d}\mathbf{x} \, \mathrm{d}t - \int_0^T \int_{\partial\Omega(t)} \left( \mu_F \frac{\partial \mathbf{v}}{\partial \mathbf{n}} - q\mathbf{n} \right) \delta \mathbf{u} \, \mathrm{d}\sigma \, \mathrm{d}t \\
& + \rho_F \int_0^T \int_{\Gamma(t)} (\delta \mathbf{u} \cdot \mathbf{v})(\mathbf{u}_S \cdot \mathbf{n}) \, \mathrm{d}\sigma \, \mathrm{d}t + \int_0^T \int_{\Gamma_D} \boldsymbol{\lambda}_F \cdot \delta \mathbf{u} \, \mathrm{d}\sigma \, \mathrm{d}t = 0 \qquad \forall \delta \mathbf{u} \in V_F(\Omega), \qquad (3.4)
\end{aligned}$$

from which we obtain the following strong form of the fluid adjoint problem:

$$\begin{cases} \rho_F \left.\dfrac{\partial \mathbf{v}}{\partial t}\right|_{\tilde{\mathcal{A}}} - \rho_F \mathbf{w}\cdot\nabla\mathbf{u} + \mu_F \Delta\mathbf{v} - \nabla q = \alpha\Delta\mathbf{u} & \text{in} \quad Q_T \\ \nabla\cdot\mathbf{v} = 0 & \text{in} \quad Q_T \\ \mathbf{v}(T) = \mathbf{0} & \text{in} \quad \Omega(T) \\ \mathbf{v} = \mathbf{0} & \text{on} \quad \Gamma_D \times (0,T) \\ \boldsymbol{\sigma}^F(\mathbf{v},q)\,\mathbf{n} = \alpha\dfrac{\partial \mathbf{u}}{\partial \mathbf{n}} & \text{on} \quad \Gamma_{\text{out}} \times (0,T); \end{cases} \tag{3.5}$$

here $(\mathbf{v}, q)$ denote the fluid adjoint variables; note that (3.5) is an unsteady Stokes problem, backward in time, written in the ALE reference coordinates after having introduced the ALE time derivative as in (2.7), according to Definition (2.4). To close the previous problem, we need to consider the following coupling conditions:

$$\begin{aligned} \mathbf{v} &= (\psi\circ\tilde{\mathcal{A}}_t^{-1})\mathbf{e}_2 && \text{on} \quad \Gamma(t)\times(0,T) \\ \rho_F(\mathbf{u}_S\cdot\mathbf{n})\mathbf{v} - \boldsymbol{\sigma}^F(\mathbf{v},q)\mathbf{n} &= -\alpha\frac{\partial\mathbf{u}}{\partial\mathbf{n}} && \text{on} \quad \Gamma(t)\times(0,T) \\ \boldsymbol{\lambda}_F &= \boldsymbol{\sigma}^F(\mathbf{v},q)\,\mathbf{n} - \alpha\frac{\partial\mathbf{u}}{\partial\mathbf{n}} && \text{on} \quad \Gamma_D\times(0,T), \end{aligned} \tag{3.6}$$

yielding the continuity of the velocity, the expression of the normal stress at the interface and the expression of the Lagrange multiplier $\boldsymbol{\lambda}_F$ used to impose the boundary conditions on the velocity, respectively.

### 3.2. Solid adjoint problem

The procedure presented in the previous section in order to write the fluid adjoint problem cannot be straightforwardly applied to derive the solid adjoint problem as well. As a matter of fact, unlike the fluid variables $(\mathbf{u}, p)$, the structure displacement $\eta$ directly affects the shape of the domain $\Omega(t)$, which is defined by

$$\Omega(t) = \{\mathbf{x}\in\mathbb{R}^2 \,:\, \mathbf{x} = \tilde{\mathcal{A}}_t(\mathbf{x}_0) \qquad \text{where} \qquad \mathbf{x}_0\in\Omega_0\}, \qquad \forall t\in(0,T); \tag{3.7}$$

where the ALE map for the case at hand is given by (2.6). Hence, we need to take into account the effect on the shape of the domain $\Omega(t)$ caused by a perturbation $\eta + \rho\delta\eta$ of the displacement, where $\rho > 0$ is a positive real parameter. Correspondingly, we denote the deformed domain by

$$\Omega_\rho(t) = \{\mathbf{S}_{\rho,t}(\mathbf{x}), \mathbf{x}\in\Omega(t)\} \qquad \rho > 0,$$

where $\mathbf{S}_{\rho,t} : \Omega(t)\to\Omega_\rho(t)$ is the harmonic extension of the field $\mathbf{x} + \rho\,\delta\eta\,\mathbf{e}_2$ defined on $\Gamma(t)$, that is,

$$\mathbf{S}_{\rho,t} = \mathbf{d}_\rho \qquad \text{where } \mathbf{d} \text{ solves} \begin{cases} -\Delta\mathbf{d}_\rho &= \mathbf{0} & \text{in} \quad \Omega(t) \\ \mathbf{d}_\rho &= \mathbf{0} & \text{on} \quad \partial\Omega(t)\setminus\Gamma(t) \\ \mathbf{d}_\rho &= \mathbf{x} + \rho\,\delta\eta\,\mathbf{e}_2 & \text{on} \quad \Gamma(t). \end{cases}$$

Let us define a vector field $\boldsymbol{\gamma}\in W^{1,\infty}(\mathbb{R}^2,\mathbb{R}^2)$ such that $\mathbf{S}_{\rho,t}(\mathbf{x}) = \mathbf{I} + \rho\boldsymbol{\gamma}(\mathbf{x})$, where $I$ denotes the identity map. Note that $\mathbf{S}_{\rho,t}$ does not depend on the map chosen to describe shape deformations during the optimization process. To characterize the expression of the solid adjoint problem, we can now require that

$$\left(\frac{\mathrm{d}}{\mathrm{d}\rho}\mathcal{L}(\mathbf{u},\eta+\rho\delta\eta,p;\mathbf{v},\psi,q;\boldsymbol{\lambda}_F,\lambda_S,\lambda_S^0,\lambda_S^1;\,\Omega)\right)\Big|_{\rho=0} = 0. \tag{3.8}$$

By introducing the displacement perturbation $I + \rho\delta\eta$, the integration domain appearing in the Lagrangian functional (3.8) is the perturbed domain $\Omega_\rho(t)$; since the fluid variables $(\mathbf{u}, p)$ are still defined on the domain $\Omega(t)$, we need to introduce a second map $\mathbf{R}_{\rho,t} = \mathbf{S}_{\rho,t}^{-1} = (\mathbf{I} + \rho\boldsymbol{\gamma})^{-1}$ and define a perturbed Lagrangian $\mathcal{L}_\rho$ to take into account the displacement perturbation and deal with properly defined variables, under the form $g_\rho = g \circ \mathbf{R}_{\rho,t}$. The perturbed Lagrangian functional $\mathcal{L}_\rho$ is thus given by

$$\begin{aligned}\mathcal{L}_\rho(\mathbf{u}, \eta + \rho\delta\eta, p; \mathbf{v}, \psi, q; \boldsymbol{\lambda}_F, \lambda_S, \lambda_S^0, \lambda_S^1;\ \Omega) = J_\rho(\mathbf{u}) - \int_0^T \int_{\Omega_\rho(t)} G(\rho)\ \mathrm{d}\mathbf{x}\,\mathrm{d}t - \int_0^T \int_0^L m(\rho)\,\mathrm{d}z\,\mathrm{d}t \\ - \int_0^T \int_{\Gamma_\rho(t)} \phi(\rho)\,\mathrm{d}\sigma\,\mathrm{d}t - \int_0^T b_F(\rho)\ \mathrm{d}t \\ - \int_0^T b_S(\rho)\,\mathrm{d}t - f_F(\rho) - \int_{\Gamma_0} f_S(\rho)\mathrm{d}\sigma, \end{aligned} \tag{3.9}$$

where:

$$J_\rho(\mathbf{u}) = \frac{\alpha}{2} \int_0^T \int_{\Omega_\rho(t)} |\nabla(\mathbf{u}_\rho)|^2\ \mathrm{d}\mathbf{x}\,\mathrm{d}t$$

represents the function cost $J$ defined on the domain $\Omega_\rho(t)$, being $\mathbf{u}_\rho = \mathbf{u} \circ \mathbf{R}_{\rho,t}$;

$$G(\rho) = -\rho_F \mathbf{u}_\rho \cdot \frac{\partial \mathbf{v}_\rho}{\partial t} - p_\rho\, \nabla \cdot \mathbf{v}_\rho + \mu_F \nabla \mathbf{u}_\rho : \nabla \mathbf{v}_\rho - q_\rho\, \nabla \cdot \mathbf{u}_\rho$$

includes the weak formulation of the fluid state equation in the Lagrangian functional, defined on the domain $\Omega_\rho(t)$;

$$m(\rho) = \rho_S h_S \frac{\partial^2(\eta + \rho\delta\eta)}{\partial t^2}\psi + \mu_S \frac{\partial(\eta + \rho\delta\eta)}{\partial x_1}\frac{\partial \psi}{\partial x_1} + \beta(\eta + \rho\delta\eta)\psi$$

is the term involving the solid state equations defined on the reference domain $\Gamma_0 = (0, L)$, where we consider the displacement perturbation $\eta$;

$$\phi(\rho) = -\rho_F(\mathbf{u}_\rho \cdot \mathbf{v}_\rho)\left(\frac{\partial(\eta + \rho\delta\eta)}{\partial t} \circ (\eta + \rho\delta\eta)^{-1}\mathbf{e}_2\right) \cdot \mathbf{n}^\rho \tag{3.10}$$

includes the terms defined on the interface $\Gamma_\rho(t)$, where $\mathbf{n}^\rho$ denotes the unit outward normal on $\Gamma_\rho(t)$;

$$b_F(\rho) = -\int_{\Gamma_D} \boldsymbol{\lambda}_{F,\rho}(\mathbf{u}_\rho - \mathbf{u}_D)\ \mathrm{d}\sigma$$

represents the Dirichlet boundary condition of the fluid state problem, defined on $\Gamma_D$;

$$b_S(\rho) = -\left[\lambda_S(\eta + \rho\delta\eta)\right]_0^L$$

results from the imposition of the Dirichlet boundary conditions of the solid state problem;

$$f_F(\rho) = \int_{\Omega_\rho(T)} \rho_F(\mathbf{u}_\rho(T) \cdot \mathbf{v}_\rho(T))\,\mathrm{d}\mathbf{x} - \rho_F \int_{\Omega_\rho(0)} \mathbf{u}_0 \cdot \mathbf{v}_\rho(0)\,\mathrm{d}\mathbf{x}$$

represents the initial and final contributions of the fluid state problem;

$$f_S(\rho) = -\lambda_S^0(\eta + \rho\delta\eta)(0) - \lambda_S^1 \frac{\partial(\eta + \rho\delta\eta)}{\partial t}(0)$$

includes the initial and the final terms of the solid state problem.
In order to derive the Lagrangian functional $\mathcal{L}_\rho$ with respect to the parameter $\rho$, we first recall two results providing the derivative of the map $\mathbf{R}_{\rho,t}$ and of a vector valued function of the form $\mathbf{u}_\rho = \mathbf{u} \circ \mathbf{R}_{\rho,t}$; see *e.g.* [38] for their proof:

**Lemma 3.1.** *Let* $\mathbf{R}_{\rho,t} : \Omega(t) \to \Omega_\rho(t)$ *be given by* $\mathbf{R}_{\rho,t} = (\mathbf{I} + \rho\,\boldsymbol{\gamma})^{-1}$; *then*

$$\left.\frac{\mathrm{d}\mathbf{R}_{\rho,t}}{\mathrm{d}\rho}\right|_{\rho=0} = -\boldsymbol{\gamma}.$$

**Lemma 3.2.** *Let* $\mathbf{R}_{\rho,t} : \Omega(t) \to \Omega_\rho(t)$ *be given by* $\mathbf{R}_{\rho,t} = (\mathbf{I} + \rho\,\boldsymbol{\gamma})^{-1}$; *then*

$$\left.\frac{\mathrm{d}\mathbf{u}_\rho}{\mathrm{d}\rho}\right|_{\rho=0} = \left.\frac{\mathrm{d}(\mathbf{u} \circ \mathbf{R}_{\rho,t})}{\mathrm{d}\rho}\right|_{\rho=0} = -\nabla\mathbf{u}\,\boldsymbol{\gamma}. \tag{3.11}$$

Since $\mathcal{L}_\rho$ depends on the parameter $\rho$ through the domain of integration as well, we take advantage of the following general result of *shape analysis* to easily express the shape derivative of functionals defined over parameter-dependent domains/boundaries; see, *e.g.*, [38, 50] for the proof:

**Theorem 3.3.** *Let* $\Omega_0 \subset \mathbb{R}^d$ *be a bounded domain locally of class* $C^2$, $\Gamma_0$ *a portion of its boundary* $\partial\Omega_0$, $\rho > 0$ *and define* $\Omega_\rho = \{\mathbf{x} \in \mathbb{R}^d \ : \ \mathbf{x} = (\mathbf{I} + \rho\boldsymbol{\gamma})\mathbf{x}_0,\ \mathbf{x}_0 \in \Omega_0\}$, $\Gamma_\rho = \{\mathbf{x} \in \mathbb{R}^d \ : \ \mathbf{x} = (\mathbf{I} + \rho\boldsymbol{\gamma})\mathbf{x}_0,\ \mathbf{x}_0 \in \Gamma_0\}$. *Then*

$$\begin{aligned}
\frac{\mathrm{d}}{\mathrm{d}\rho}\left(\int_{\Omega_\rho} y(\rho)\,\mathrm{d}\mathbf{x}\right)\bigg|_{\rho=0} &= \int_{\Omega_0} \left.\frac{\partial y(\rho)}{\partial\rho}\right|_{\rho=0} \mathrm{d}\mathbf{x} + \int_{\partial\Omega_0} y(0)(\boldsymbol{\gamma}\cdot\mathbf{n})\mathrm{d}\sigma,\\
\frac{\mathrm{d}}{\mathrm{d}\rho}\left(\int_{\Gamma_\rho} y(\rho)\mathrm{d}\sigma\right)\bigg|_{\rho=0} &= \int_{\Gamma_0} \left(y'(0) + \left(H\,y(0) + \frac{\partial y(0)}{\partial \boldsymbol{n}}\right)(\boldsymbol{\gamma}\cdot\mathbf{n})\right)\mathrm{d}\sigma,
\end{aligned} \tag{3.12}$$

*where* $H = \nabla\cdot\mathbf{n}$ *is the mean curvature of* $\Gamma_0$.

A further result we have proved (see Appendix 6) is required to derive the term involving the function $\phi(\rho)$ defined in (3.10):

**Lemma 3.4.** *Let* $\phi(\rho)$ *be the function defined in* (3.10), *then the following identity holds*:

$$\begin{aligned}
\frac{\mathrm{d}}{\mathrm{d}\rho}\left(\int_0^T\int_{\Gamma_\rho(t)}\phi(\rho)\mathrm{d}\sigma\right)\bigg|_{\rho=0} &= \rho_F\int_0^T\int_{\Gamma(t)}\left(\frac{\partial\mathbf{u}}{\partial t}\cdot\mathbf{v} + \frac{\partial\mathbf{v}}{\partial t}\cdot\mathbf{u}\right)(\boldsymbol{\gamma}\cdot\mathbf{n})\mathrm{d}\sigma\,\mathrm{d}t\\
&+\rho_F\int_0^T\int_{\Gamma(t)}[(\mathbf{u}\cdot\mathbf{v})((\nabla_{\Gamma(t)}\mathbf{n} + \mathbf{N})\,\mathbf{u}_S)\cdot\boldsymbol{\gamma}]\mathrm{d}\sigma\,\mathrm{d}t - \rho_F\int_{\Gamma(T)}(\mathbf{u}\cdot\mathbf{v})(T)(\boldsymbol{\gamma}\cdot\mathbf{n})\mathrm{d}\sigma\\
&+\rho_F\int_{\Gamma_0}(\mathbf{u}_0\cdot\mathbf{v}(0))(\boldsymbol{\gamma}\cdot\mathbf{n})\mathrm{d}\sigma + \rho_F\int_0^T\int_{\Gamma(t)}[(\nabla\mathbf{u}\,\boldsymbol{\gamma})\cdot\mathbf{v} + (\nabla\mathbf{v}\,\boldsymbol{\gamma})\cdot\mathbf{u}]\,(\mathbf{u}_S\cdot\mathbf{n})\mathrm{d}\sigma\,\mathrm{d}t
\end{aligned}$$

*where* $\nabla_{\Gamma(t)}\mathbf{n}$ *denotes the tangential gradient of* $\mathbf{n} = (n_1, n_2)^T$ *in* $\Gamma(t)$ *and* $\mathbf{N}$ *the diagonal matrix defined as follows:* $N_{ij} = n_i\delta_{ij}$, *where* $\delta_{ij}$ *denotes the Kronecker delta.*

By using Theorem 3.3, Lemmas 3.2 and 3.4, we can now calculate the derivative (3.8) of the Lagrangian functional with respect to the parameter $\rho$:

$$\begin{aligned}\left.\frac{\mathrm{d}\,\mathcal{L}_\rho}{\mathrm{d}\rho}\right|_{\rho=0} &= A_\Omega + \frac{\alpha}{2}\int_0^T\int_{\Gamma(t)} |\nabla\mathbf{u}|^2(\boldsymbol{\gamma}\cdot\mathbf{n})\mathrm{d}\sigma\,\mathrm{d}t + \rho_F\int_0^T\int_{\Gamma(t)}(\mathbf{u}\cdot\mathbf{v})(\mathbf{W}_0\cdot\mathbf{n})\mathrm{d}\sigma\,\mathrm{d}t\\ &- \int_0^T\int_{\Gamma(t)}\left[-\rho_F\frac{\partial\mathbf{v}}{\partial t}\cdot\mathbf{u} - p\,\nabla\cdot\mathbf{v} + \mu_F\nabla\mathbf{u}:\nabla\mathbf{v} - q\,\nabla\cdot\mathbf{u}\right](\boldsymbol{\gamma}\cdot\mathbf{n})\mathrm{d}\sigma\mathrm{d}t\\ &+ \int_0^T\int_{\Gamma(t)}\nabla\cdot(\rho_F(\mathbf{u}\cdot\mathbf{v})\mathbf{u}_S)(\boldsymbol{\gamma}\cdot\mathbf{n})\mathrm{d}\sigma\,\mathrm{d}t\\ &- \rho_F\int_0^T\int_{\Gamma(t)}\left[(\nabla\mathbf{u}\,\boldsymbol{\gamma})\cdot\mathbf{v} + (\nabla\mathbf{v}\,\boldsymbol{\gamma})\cdot\mathbf{u}\right](\mathbf{u}_S\cdot\mathbf{n})\mathrm{d}\sigma\,\mathrm{d}t\\ &- \int_{\Gamma(T)}\rho_F(\mathbf{u}(T)\cdot\mathbf{v}(T))(\boldsymbol{\gamma}\cdot\mathbf{n})\mathrm{d}\sigma + \rho_F\int_{\Gamma_0}(\mathbf{u}_0\cdot\mathbf{v}(0))(\boldsymbol{\gamma}\cdot\mathbf{n})\mathrm{d}\sigma + \int_0^T\left[\lambda_S\delta\eta\right]_0^L\mathrm{d}t\\ &- \int_0^T\int_0^L\left(\rho_S h_S\frac{\partial^2\delta\eta}{\partial t^2}\psi + \mu_S\frac{\partial\psi}{\partial x_1}\frac{\partial\delta\eta}{\partial x_1} + \beta\psi\right)\mathrm{d}x_1\,\mathrm{d}t + \int_0^L\left(\lambda_S^0\delta\eta(0) + \lambda_S^1\frac{\partial\delta\eta}{\partial t}(0)\right)\mathrm{d}x_1. \end{aligned}\tag{3.13}$$

where

$$\begin{aligned}A_\Omega = &-\alpha\int_0^T\int_{\Omega(t)}\nabla\mathbf{u}:\nabla(\nabla\mathbf{u}\,\boldsymbol{\gamma})\,\mathrm{d}\mathbf{x}\,\mathrm{d}t - \int_0^T\int_{\Omega(t)}\rho_F\left[\frac{\partial\mathbf{v}}{\partial t}\cdot(\nabla\mathbf{u}\,\boldsymbol{\gamma}) + \mathbf{u}\cdot\frac{\partial(\nabla\mathbf{v}\boldsymbol{\gamma})}{\partial t}\right]\mathrm{d}\mathbf{x}\,\mathrm{d}t\\ &- \int_0^T\int_{\Omega(t)}\left[p\,\nabla\cdot(\nabla\mathbf{v}\,\boldsymbol{\gamma}) + (\nabla p\cdot\boldsymbol{\gamma})\nabla\cdot\mathbf{v}\right]\mathrm{d}\mathbf{x}\,\mathrm{d}t + \mu_F\int_0^T\int_{\Omega(t)}\left[\nabla(\nabla\mathbf{v}\,\boldsymbol{\gamma}):\nabla\mathbf{u} + \nabla\mathbf{v}:\nabla(\nabla\mathbf{u}\,\boldsymbol{\gamma})\right]\mathrm{d}\mathbf{x}\,\mathrm{d}t\\ &+ \rho_F\int_{\Omega(T)}\left[(\nabla\mathbf{u}\,\boldsymbol{\gamma})\cdot\mathbf{v} + (\nabla\mathbf{v}\,\boldsymbol{\gamma})\cdot\mathbf{u}\right](T)\,\mathrm{d}\mathbf{x} - \rho_F\int_{\Omega_0}\mathbf{u}_0\cdot(\nabla\mathbf{v}\,\boldsymbol{\gamma})(0)\,\mathrm{d}\mathbf{x}\\ &- \int_0^T\int_{\Gamma_D}\left(\boldsymbol{\lambda}_F\cdot(\nabla\mathbf{u}\,\boldsymbol{\gamma}) + (\nabla\boldsymbol{\lambda}_F\,\boldsymbol{\gamma})\cdot(\mathbf{u}-\mathbf{u}_D)\right)\mathrm{d}\sigma\mathrm{d}t. \end{aligned}\tag{3.14}$$

A further simplification of the term $A_\Omega$ is possible thanks to the following result, whose proof is reported in Appendix 6:

**Lemma 3.5.** *Let $A_\Omega$ be the functional defined in (3.14), then the following identity holds*:

$$A_\Omega = \int_0^T\int_{\Gamma(t)}\left(\rho_F(\mathbf{u}_S\cdot\mathbf{n})(\mathbf{u}\cdot(\nabla\mathbf{v}\,\boldsymbol{\gamma}) + (\nabla\mathbf{u}\,\boldsymbol{\gamma})\cdot\mathbf{v}\right)\mathrm{d}\sigma\,\mathrm{d}t + \int_0^T\int_{\Gamma(t)}(\boldsymbol{\sigma}^F(\mathbf{u},p)\,\mathbf{n})\cdot(\nabla\mathbf{v}\,\boldsymbol{\gamma})\,\mathrm{d}\sigma\,\mathrm{d}t.$$

Thanks to this lemma, the expression of the derivative (3.13) of the Lagrangian functional is given by:

$$\begin{aligned}\left.\frac{\mathrm{d}\mathcal{L}}{\mathrm{d}\rho}\right|_{\rho=0} &= \frac{\alpha}{2}\int_0^T\int_{\Gamma(t)}|\nabla\mathbf{u}|^2(\boldsymbol{\gamma}\cdot\mathbf{n})\,\mathrm{d}\sigma\,\mathrm{d}t - \rho_F\int_0^T\int_{\Gamma(t)}(\mathbf{u}\cdot\mathbf{v})((\nabla_{\Gamma(t)}\mathbf{n}+\mathbf{N})\,\mathbf{u}_S)\cdot\boldsymbol{\gamma}\,\mathrm{d}\sigma\,\mathrm{d}t\\ &-\rho_F\int_0^T\int_{\Gamma(t)}\left(\frac{\partial\mathbf{u}}{\partial t}\cdot\mathbf{v}\right)(\boldsymbol{\gamma}\cdot\mathbf{n})\,\mathrm{d}\sigma\,\mathrm{d}t + \int_0^L\left(\lambda_S^0\delta\eta(0) + \lambda_S^1\frac{\partial\delta\eta}{\partial t}(0)\right)\mathrm{d}x_1\\ &- \int_0^T\int_0^L\left(\rho_S h_S\frac{\partial^2\delta\eta}{\partial t^2}\psi + \mu_S\frac{\partial\psi}{\partial x_1}\frac{\partial\delta\eta}{\partial x_1} + \beta\psi\right)\mathrm{d}x_1\,\mathrm{d}t + \int_0^T\left[\lambda_S\delta\eta\right]_0^L\mathrm{d}t. \end{aligned}\tag{3.15}$$

Finally, by requiring that at the optimum this derivative is vanishing – so that condition (3.8) holds – yields the following solid adjoint problem under strong form:

$$\begin{cases}\rho_S h_S\dfrac{\partial^2\psi}{\partial t^2} - \mu_S\dfrac{\partial^2\psi}{\partial x_1^2} + \beta\psi = g(t) & \text{on} \quad \Gamma_0\times(0,T)\\ \psi(0,t) = \psi(L,t) = 0 & t\in(0,T)\\ \psi(x_1,T) = \dfrac{\partial\psi}{\partial t}(x_1,T) = 0 & \mathbf{x}\in\Gamma_0, \end{cases}\tag{3.16}$$

where $g$ is defined as follows, for any $t \in (0,T)$:

$$g(t) = \left( \frac{\alpha}{2} |\nabla \mathbf{u}|^2 \, n_2 - \rho_F \left( \frac{\partial \mathbf{u}}{\partial t} \cdot \mathbf{v} \right) n_2 - \rho_F (\mathbf{u} \cdot \mathbf{v})((\nabla_\Gamma \mathbf{n} + \mathbf{N}) \, \mathbf{u}_S) \cdot \mathbf{e}_2 \right) \Big|_{\Gamma(t)} \circ \eta^{-1}. \tag{3.17}$$

Problem (3.16) yields nothing but the expression of a linear Koiter model backward in time, for the adjoint displacement $\psi$. This problem depends on the solution $(\mathbf{u}, p, \eta)$ of the state FSI problem and on the fluid adjoint variables $(\mathbf{v}, q)$. We also point out that the fluid and the solid adjoint problems are coupled, thanks to conditions (3.6) and (3.17) which, similarly to the case of the state FSI problem, impose the continuity of both velocity and stress, respectively, on the interface $\Gamma(t)$. Moreover, by requiring that at the optimum the derivative in (3.15) vanishes, we get the following expressions for the Lagrangian multipliers $\lambda_S \in L^2(0,T)$, $\lambda_S^0 \in L^2(\Gamma_D)$ and $\lambda_S^1 \in L^2(\Gamma_D)$:

$$\lambda_S = -\mu_S \frac{\partial \psi}{\partial z} \text{ on } (\{0\} \cup \{L\}) \times (0,t) \qquad \lambda_S^0 = -\frac{\partial \psi}{\partial t}(0) \qquad \text{and} \qquad \lambda_S^1 = \psi(0) \qquad \text{on} \qquad \Gamma_0 \times \{0\}.$$

### 3.3. Shape derivative of the cost functional

The last quantity to derive in order to set a system of first-order necessary optimality condition is the shape derivative of the cost functional $J$ (or, equivalently, of its shape gradient). Together with the state and the adjoint problems, the shape gradient of $J$ is indeed required to characterize the solution to the shape optimization problem and, from a practical standpoint, to set up a descent method for its numerical approximation.

According to the Lagrangian multipliers method, we can treat the state and the adjoint variables as independent from the domain $\Omega(t)$ and, therefore, we can derive the Lagrangian functional $\mathcal{L}$ with respect to the shape in order to evaluate the shape derivative of the cost functional $J$. This is achieved by applying, to the case at hand, two classical results of shape analysis, which we report for the sake of completeness (see, *e.g.* ([1] for the proof), Props. 6.22, 6.24):

**Theorem 3.6.** *Let $\Omega_0 \subset \mathbb{R}^n$ be a bounded domain locally of class $\mathcal{C}^2$, $f \in W^{1,1}(\mathbb{R}^n)$ and $g \in W^{2,1}(\mathbb{R}^n)$. Denote by $\mathbf{n}$ the unit outward normal on $\partial\Omega_0$ and by $H = \nabla \cdot \mathbf{n}$ the mean curvature of $\partial\Omega_0$. Then*:

(1) *the functional $J(\Omega) = \int_\Omega f(\mathbf{x}) \mathrm{d}\mathbf{x}$ is differentiable in $\Omega_0$ and*

$$J'(\Omega_0)(\boldsymbol{\theta}) = \int_{\partial\Omega_0} (\boldsymbol{\theta} \cdot \mathbf{n}) f \, \mathrm{d}\sigma \qquad \forall \boldsymbol{\theta} \in W^{1,\infty}(\mathbb{R}^n; \mathbb{R}^n);$$

(2) *the functional $J(\Omega) = \int_{\partial\Omega} g(\mathbf{x}) \mathrm{d}\sigma$ is differentiable in $\Omega_0$ and*

$$J'(\Omega_0)(\boldsymbol{\theta}) = \int_{\partial\Omega_0} (\boldsymbol{\theta} \cdot \mathbf{n}) \left( \frac{\partial g}{\partial \mathbf{n}} + Hg \right) \mathrm{d}\sigma \qquad \forall \theta \in W^{1,\infty}(\mathbb{R}^n; \mathbb{R}^n).$$

Applying the results above, it is possible to calculate the derivative of the Lagrangian functional $\mathcal{L}$ defined by (3.1) with respect to the domain, evaluated at $\hat{\Omega}$ in the direction of $\boldsymbol{\theta} \in W^{1,\infty}(\mathbb{R}^2, \mathbb{R}^2)$. Let us assume that $\Gamma_M \subseteq \Gamma_b$ is the only boundary portion on which we can act during the optimization process; then, the admissible displacement fields are such that

$$\boldsymbol{\theta} \in \boldsymbol{\Theta} = \{ \boldsymbol{\theta} \in W^{1,\infty}(\mathbb{R}^2, \mathbb{R}^2) \ : \ \boldsymbol{\theta} = \mathbf{0} \qquad \text{on} \qquad \partial\Omega_0 \setminus \Gamma_M \} \tag{3.18}$$

Thus, for any $\boldsymbol{\theta} \in \boldsymbol{\Theta}$, the shape derivative of the cost functional $J$ defined by (2.11) reads as follows:

$$J'(\Omega_0)(\boldsymbol{\theta}) = \left\langle \frac{\partial \mathcal{L}}{\partial \Omega_0}, \boldsymbol{\theta} \right\rangle = \int_0^T \int_{\Gamma_M} \left( H\, \boldsymbol{\lambda}_F \cdot (\mathbf{u} - \mathbf{u}_D) + \frac{\partial (\boldsymbol{\lambda}_F \cdot (\mathbf{u} - \mathbf{u}_D))}{\partial \mathbf{n}} \right) (\boldsymbol{\theta} \cdot \mathbf{n}) \mathrm{d}\sigma \, \mathrm{d}t + \int_0^T \int_{\Gamma_M} \left( \frac{\alpha}{2} |\nabla \mathbf{u}|^2 + \rho_F \mathbf{u} \cdot \frac{\partial \mathbf{v}}{\partial t} - \mathbf{v} \cdot \nabla p + \mu_F \Delta \mathbf{u} \cdot \mathbf{v} + q \nabla \cdot \mathbf{u} \right) (\boldsymbol{\theta} \cdot \mathbf{n}) \mathrm{d}\sigma \, \mathrm{d}t \tag{3.19}$$

By exploiting the boundary conditions $\mathbf{u} = \mathbf{v} = \mathbf{0}$ on $\Gamma_b$ of the state and adjoint problems and recalling the expression (3.6) of the Lagrange multiplier $\boldsymbol{\lambda}_F$, the shape derivative $J'(\Omega_0)(\boldsymbol{\theta})$ takes the following form:

$$\begin{aligned} J'(\Omega_0)(\boldsymbol{\theta}) &= \int_0^T \int_{\Gamma_M} \left( \frac{\alpha}{2} |\nabla \mathbf{u}|^2 + \frac{\partial ((\boldsymbol{\sigma}^F(\mathbf{v}, q)\, \mathbf{n} - \alpha \nabla \mathbf{u}\, \mathbf{n}) \cdot \mathbf{u})}{\partial \mathbf{n}} \right) (\boldsymbol{\theta} \cdot \mathbf{n}) \, \mathrm{d}\sigma \, \mathrm{d}t \\ &= \mu_F \int_0^T \int_{\Gamma_M} (\nabla \mathbf{u} : \nabla \mathbf{v})(\boldsymbol{\theta} \cdot \mathbf{n}) \mathrm{d}\sigma \, \mathrm{d}t - \frac{\alpha}{2} \int_0^T \int_{\Gamma_M} |\nabla \mathbf{u}|^2 (\boldsymbol{\theta} \cdot \mathbf{n}) \, \mathrm{d}\sigma \, \mathrm{d}t. \end{aligned} \tag{3.20}$$

See, *e.g.*, [6] for further details on how to recover (3.20) from (3.19).

Hence, we require that the optimal shape fulfills the following optimality condition (which is nothing but the expression of a *minimum principle* for the shape optimization problem at hand):

$$J'(\hat{\Omega})(\boldsymbol{\theta}) \geq 0 \qquad \forall \boldsymbol{\theta} \in \boldsymbol{\Theta}.$$

We point out that, for a generic domain $\Omega_0$, the shape derivative can be equivalently expressed as follows:

$$J'(\Omega_0)(\boldsymbol{\theta}) = \langle \nabla J(\Omega_0), \boldsymbol{\theta} \rangle \qquad \text{where} \qquad \nabla J(\Omega_0) = \left[ \mu_F \nabla \mathbf{u}(\Omega_0) \, : \, \nabla \mathbf{v}(\Omega_0) - \frac{\alpha}{2} |\nabla \mathbf{u}(\Omega_0)|^2 \right] \mathbf{n}$$

where $\nabla J = \nabla J(\Omega_0)$ is the *shape gradient* of $J$ evaluated at $\Omega_0$. As we will see in the following section, evaluating this quantity (once the state and the adjoint problems have been solved) is a cornerstone in order to setup a suitable descent method for the solution solution to the shape optimization problem.

We can summarize all the results presented in this section in the following

**Theorem 3.7.** *Let us consider the shape optimization problem* (2.10)–(2.12)*. Then, the shape derivative of the cost functional $J(\Omega)$ defined in* (2.11)*, for any $\Omega \in \mathcal{O}_{ad}$, is given by*

$$J'(\Omega)(\boldsymbol{\theta}) = \mu_F \int_0^T \int_{\Gamma_M} (\nabla \mathbf{u} : \nabla \mathbf{v})(\boldsymbol{\theta} \cdot \mathbf{n}) \mathrm{d}\sigma \, \mathrm{d}t - \frac{\alpha}{2} \int_0^T \int_{\Gamma_M} |\nabla \mathbf{u}|^2 (\boldsymbol{\theta} \cdot \mathbf{n}) \, \mathrm{d}\sigma \, \mathrm{d}t. \tag{3.21}$$

*where $(\mathbf{u}, p, \eta)$ fulfill the fluid state problem* (2.7)*, the solid state problem* (2.2) *and the coupling conditions* (2.8)*; $(\mathbf{v}, q, \psi)$ fulfill the fluid adjoint problem* (3.5)*, the solid adjoint problem* (3.16) *and the coupling conditions* (3.6)*.*

## 4. Numerical approximation

In this section we describe a numerical procedure to approximate the shape optimization problem we have analyzed so far, based on the system of optimality conditions we have derived. First, we recall how to solve the state FSI problem relying on a Dirichlet−Neumann approach; then, we suitably modify this method to tackle the solution to the adjoint problem backward in time; at last, we describe a steepest descent-like method to address the optimization problem. We recall that we rely on an *optimize-then-discretize* approach, thus discretizing (both in space and time) the system of optimality conditions derived so far. We first focus on the time discretization with finite differences, then we provide some details about the spatial discretization operated through a finite element method.

### 4.1. Numerical approximation of the FSI state problem

By exploiting the low dimension of the structural problem, it is possible to describe an efficient iterative procedure (see Algorithm 1) to solve the FSI problem, where the coupling conditions are imposed at the interface $\Gamma(t)$ through a Dirichlet−Neumann approach. In particular, at each time step, we solve iteratively, until a suitable stopping criterion is satisfied,

- a fluid sub-problem where the velocity continuity on $\Gamma(t)$ is imposed as a Dirichlet condition;
- a solid sub-problem where the stress continuity on $\Gamma(t)$ is imposed as a Neumann condition.

Let us consider a partition of the time interval $[0, T]$ in $N$ subintervals, where $t^n = n\Delta t$, $n = 0, \dots, N$, $\Delta t$ is a fixed time step and $t^N = T$. Then, let us denote by $g^n$ the value of the function $g(\cdot, t)$ at $t = t^n$ and by $g_j$ the value of the function $g(\cdot, t)$ at the $j$-th iteration of the FSI iterative scheme. Furthermore, let us consider a suitable approximation of the reference solid domain $\Gamma_0$. For the time discretization, we employ a first-order backward difference scheme for the structure and an implicit Euler scheme for the fluid. The numerical approximation of the state FSI problem is as follows. Given a fixed tolerance $\tau$, an initial displacement $\eta^0$, let us initialize the value of the displacement in the FSI iterative process as follows: $\eta_0 = \eta^0$. Thus, for each time step $n = 1, \dots, N$ we need to (see Algorithm 1):

- given $(\mathbf{u}^n, p^n, \eta^n)$, the configuration $\Omega^n = \Omega(t^n)$ whose boundary is $\Gamma^n = \Gamma(t^n)$, solve the fluid sub-problem: find $(\mathbf{u}_j, p_j)$ such that:

$$\begin{cases} \rho_F \dfrac{\mathbf{u}_j - \mathbf{u}^n}{\Delta t} - \rho_F \mathbf{w}^n \cdot \nabla \mathbf{u}_j + \nabla p_j - \mu_F \Delta \mathbf{u}_j = 0 & \text{in} \quad \Omega^n \\ \nabla \cdot \mathbf{u}_j = 0 & \text{in} \quad \Omega^n \\ \mathbf{u}_j = \left( \left( \dfrac{\eta_{j-1} - \eta^n}{\Delta t} \right) \circ \tilde{\mathcal{A}}_t^{-1} \right) \Big|_{\Gamma^n} \cdot \mathbf{e}_2 & \text{on} \quad \Gamma^n \\ \mathbf{u}_j = \mathbf{u}_{\text{in}}^n & \text{on} \quad \Gamma_{\text{in}} \\ \mathbf{u}_j = \mathbf{0} & \text{on} \quad \Gamma_b \\ -p_j \mathbf{n}^n + \nu \dfrac{\partial \mathbf{u}_j}{\partial \mathbf{n}^n} = \mathbf{0} & \text{on} \quad \Gamma_{\text{out}}\,; \end{cases} \tag{4.1}$$

- solve the solid sub-problem: find $\tilde{\eta}_j$ such that:

$$\begin{cases} \rho_S h_S \dfrac{\tilde{\eta}_j - 2\eta^n + \eta^{n-1}}{\Delta t^2} - \mu_S \dfrac{\partial^2 \tilde{\eta}_j}{\partial x_1^2} + \beta \tilde{\eta}_j = f_j & \text{on} \quad (0, L) \\ f_j = -\mathcal{J}^n \left( \boldsymbol{\sigma}^F(\mathbf{u}_j, p_j)\, \mathbf{n}^n \right) \big|_{\Gamma^n} \cdot \mathbf{e}_2 & \text{on} \quad (0, L) \\ \tilde{\eta}_j(0) = \tilde{\eta}_j(L) = 0\,; \end{cases} \tag{4.2}$$

- update the structure according to a relaxation parameter $\gamma \in (0, 1)$, as follows:

$$\eta_j = \gamma \tilde{\eta}_j + (1 - \gamma) \eta_{j-1}; \tag{4.3}$$

- perform a convergence test: if $\|\eta_j - \eta_{j-1}\|_{L^2(0,L)} < \tau$, then set $\eta^{n+1} = \eta_j$ and $\mathbf{u}^{n+1} = \mathbf{u}_j$; otherwise, set $j = j + 1$ and go back to step 1.

At the end of each time step, the domain $\Omega^n$ is deformed into the domain $\Omega^{n+1}$, by exploiting the weak solution $\eta^{n+1}$ of the solid sub-problem. Note that the velocity $\mathbf{w}^n$ of the domain $\Omega^n$ can be numerically approximated by doing an harmonic extension onto the whole $\Omega^n$ of the vector $(\mathbf{u}^n \cdot \mathbf{e}_2)\mathbf{e}_2$ defined in $\Gamma^n$, similarly to what done in (2.6) – recall the identity (2.9). A schematic description of the whole procedure is provided in Algorithm 1, Appendix 6.

We point out that the fluid sub-problem (4.1) at $t = t^{n+1}$ is solved in the fixed domain $\Omega^n$. Moreover, unlike the continuous formulation of the FSI problem, which is nonlinear because of the coupling conditions

and the definition of the domain $\Omega(t)$, the fluid sub-problem (4.1) and the solid sub-problem (4.2) are linear in their arguments. Furthermore, a really important step in the procedure above is represented by the relaxation step (4.3) for the structure updating. As a matter of fact, it can be proved [9,18] that there exists $\bar{\gamma} < 1$, such as, for $\gamma < \bar{\gamma}$, the Dirichlet−Neumann procedure above converges to the solution of the time-discrete FSI problem.

The procedure above can be easily modified in order to solve the adjoint FSI problem as well, by recalling that (i) both the fluid and the solid adjoint problems are backward in time, with initial conditions at $t = T$, and (ii) the domains $\Omega^n$ now are known by the solution to the state FSI problem. Hence, given a fixed tolerance $\tau > 0$, the solution to the state FSI problem at $t^n$ $(\mathbf{u}^n, p^n, \eta^n; \Omega^n)$ and the solution to the adjoint problem at $t^{n+1}$ $(\mathbf{v}^{n+1}, q^{n+1}, \psi^{n+1})$, to solve the FSI adjoint problem at $t^n$, we need, for each $j = 1, \ldots, N$, to (see Algorithm **2**, Appendix 6):

– solve the fluid adjoint sub-problem: find $(\mathbf{v}_j, q_j)$ such that:

$$\begin{cases} \rho_F \dfrac{\mathbf{v}^{n+1} - \mathbf{v}_j}{\Delta t} - \rho_F \mathbf{w}^n \cdot \nabla \mathbf{v}_j - \nabla q_j + \mu_F \Delta \mathbf{v}_j = \alpha \Delta \mathbf{u}^n & \text{in} \quad \Omega^n \\ \nabla \cdot \mathbf{v}_j = 0 & \text{in} \quad \Omega^n \\ \mathbf{v}_j = \left( \psi_{j-1} \circ \tilde{\mathcal{A}}_t^{-1} \right)\Big|_{\Gamma^n} \cdot \mathbf{e}_2 & \text{on} \quad \Gamma^n \\ \mathbf{v}_j = \mathbf{0} & \text{on} \quad \Gamma_{\text{in}} \cup \Gamma_b \\ -q_j \mathbf{n}^n + \nu \dfrac{\partial \mathbf{v}_j}{\partial \mathbf{n}^n} = \mathbf{0} & \text{on} \quad \Gamma_{\text{out}} ; \end{cases} \tag{4.4}$$

– solve the solid adjoint sub-problem: find $\tilde{\psi}_j$ such that:

$$\begin{cases} \rho_S h_S \dfrac{\tilde{\psi}_j - 2\eta^{n+1} + \eta^{n+2}}{\Delta t^2} - \mu_S \dfrac{\partial^2 \tilde{\psi}_j}{\partial x_1^2} + \beta \tilde{\psi}_j = g_j \quad \text{on} \quad (0, L) \\ \tilde{\psi}_j(0) = \tilde{\psi}(L) = 0 \end{cases} \tag{4.5}$$

where $g_j$ is the $L^2$-projection of the forcing term $g$ of the solid adjoint problem, defined in (3.17);

– update the structure according to a *relaxation parameter* $\omega \in (0, 1)$ as follows:

$$\psi_j = \omega \, \tilde{\psi}_j + (1 - \omega) \, \psi_{j+1} ; \tag{4.6}$$

– perform a convergence test: if $\|\psi_j - \psi_{j-1}\|_{L^2(0,L)} < \tau$, then set $\psi^n = \psi_j$ and $\mathbf{v}^n = \mathbf{v}_j$; otherwise, set $j = j + 1$ and go back to step 1.

**Remark 4.1.** A generalization of the Dirichlet−Neumann scheme exploited for the case at hand is provided by the Robin−Robin partitioned procedure, introduced in [4,5] and analyzed in [22]; such a technique avoids the relaxation and shows better convergence properties in the presence of a high added-mass; another option would be the Robin-Neumann scheme, which in [4,5] has been shown to converge without relaxation. The choice of the parameters in the Robin transmission conditions is a key factor in order to enhance the convergence properties of the Robin−Robin scheme, and can be made by either heuristic considerations [4, 5] of through a suitable optimization procedure [22]. Although relying on such a scheme in view of more complex applications (such as those, *e.g.*, related to shape optimization problems involving Navier-Stokes flows and FSI effects) is somehow required, for the case at hand we opted for a Dirichlet−Neumann scheme, easier to implement and yet capable to provide satisfying results entailing reasonable computational costs.

Algorithms **1** and **2** in Appendix 6 provide the time approximation of the state and the adjoint equation, respectively. In order to obtain the fully discrete solution, we consider a space approximation of these problems by means of the Galerkin−Finite Element (FE) method; for the sake of simplicity, we limit ourselves to the state problem, the treatment of the adjoint problem being indeed very similar. In particular, denoting by $h$ the

mesh size, let us introduce two meshes $\mathcal{T}_h^{F,n}$, $\mathcal{T}_h^S$, approximating respectively the fluid domain $\Omega^n$ and the solid domain $\Gamma_0 = (0, L)$ by nonoverlapping triangles or segment. Moreover, let us introduce the FE spaces

$$X_h^n = \left\{ \mathbf{v}_h \in C^0(\Omega^n; \mathbb{R}^2) : \mathbf{v}_h|_{K^F} \in \mathbb{P}_r,\ \forall K^F \in \mathcal{T}_h^{F,n} \right\},$$
$$Y_h^n = \left\{ q_h \in C^0(\Omega^n) : q_h|_{K^F} \in \mathbb{P}_l,\ \forall K^F \in \mathcal{T}_h^{F,n} \right\} \quad , \quad Z_h = \left\{ \xi_h \in C^0(0, L) : \xi_h|_{K^S} \in \mathbb{P}_k,\ \forall K^S \in \mathcal{T}_h^S \right\},$$

where $r, l, k$ denote the degrees of the polynomials approximating the variables $\mathbf{u}, p, \eta$, and $\mathbb{P}_r$ the space of the polynomials with global degrees equal or lower than $r$. Finally, let us denote by $V_h^{F,n} \subset X_h^{F,n} \cap V_F(\Omega^n), Q_h^n \subset Y_h^n \cap Q_F(\Omega^n), V_h^S \subset Z_h^k \cap V_S$ and $V_{h,0}^{F,n} = X_h^{F,n} \cap V_0(\Omega^n)$, in which homogeneous Dirichlet conditions are imposed. By introducing the variables $\mathbf{u}_h \in V_h^{F,n}, p_h \in Q_h^n$ and $\eta_h \in V_h^S$ approximating $\mathbf{u}_j, p_j, \tilde{\eta}_j$, respectively, the Galerkin−FE approximation of problems (4.1), (4.2) read as follows:

- given the velocity $\mathbf{w}_h^n$ of the computational domain and the solution $\mathbf{u}_h^n$ evaluated in $t^n$, find $\mathbf{u}_h \in V_h^{F,n}$ and $p_h \in Q_h^n$ such that $\mathbf{u}_h^n|_{\Gamma^n}$ fulfills the Dirichlet boundary conditions in (4.1) and

$$\begin{aligned} &\rho_F \int_{\Omega^n} \frac{\mathbf{u}_h - \mathbf{u}_h^n}{\Delta t} \cdot \boldsymbol{\varphi}_h \, \mathrm{d}\mathbf{x} - \rho_F \int_{\Omega^n} [(\mathbf{w}_h^n \cdot \nabla)\mathbf{u}_h] \cdot \boldsymbol{\varphi}_h \, \mathrm{d}\mathbf{x} \\ &\qquad - \int_{\Omega^n} p_h \, \nabla \cdot \boldsymbol{\varphi}_h \mathrm{d}\mathbf{x} + \mu_F \int_{\Omega^n} \nabla \mathbf{u}_h : \nabla \boldsymbol{\varphi}_h \, \mathrm{d}\mathbf{x} = 0 \quad \forall \boldsymbol{\varphi}_h \in V_{h,0}^{F,n}, \\ &\int_{\Omega^n} \phi_h \, \nabla \cdot \mathbf{u}_h \, \mathrm{d}\mathbf{x} \qquad\qquad \forall \phi_h \in Q_h^n; \end{aligned} \tag{4.7}$$

- given the approximation $f_h^{n+1}$ of the forcing term $f$ defined in the coupling condition (2.8), and the numerical solutions $\eta_h^n$ and $\eta_h^{n-1}$, find $\eta_h \in V_h^S$ such that $\eta_h(0) = \eta_h(L) = 0$ and

$$\rho_S h_s \int_{\Gamma_0} \frac{\eta_h - 2\eta_h^n + \eta_h^{n-1}}{\Delta t^2} \xi_h \, \mathrm{d}x_1 + \mu_S \int_{\Gamma_0} \frac{\partial \eta_h}{\partial x_1} \frac{\partial \xi_h}{\partial x_1} \mathrm{d}x_1 + \beta \int_{\Gamma_0} \eta_h \xi_h \, \mathrm{d}x_1 = \int_{\Gamma_0} f_h^{n+1} \xi_h \mathrm{d}x_1 \quad \forall \xi_h \in V_h^S. \tag{4.8}$$

Further details about the algebraic formulation of these problems are provided in Appendix 6.

### 4.2. Numerical approximation of the optimization problem

We are now ready to combine all the methods described so far in order to set up a numerical procedure for the solution to our shape optimization problem. To compute the optimal shape, we rely on a descent method based on the shape gradient of the cost functional; see, *e.g.*, [1,25] for further details. In particular, let us denote by $g^{(k)}$ the value of the generic function $g(\cdot)$ evaluated at the $k$-th iteration of the optimization scheme. Thus, starting from an initial configuration $\Omega^{(0)}$ of the domain, at each step $k = 0, 1, \ldots$ of the descent algorithm we need to:

(a) solve the state problem, by setting $\Omega(0) = \Omega^{(k)}$, to compute $\mathbf{y}_h^{(k)} = (\mathbf{u}_h^{(k)}, p_h^{(k)}, \eta_h^{(k)})$;
(b) evaluate the cost functional $J_h(\Omega^{(k)}) = J(\Omega^{(k)}, \mathbf{y}_h^{(k)})$;
(c) solve the adjoint problem to compute $\mathbf{z}_h^{(k)} = (\mathbf{v}_h^{(k)}, q_h^{(k)}, \psi_h^{(k)})$;
(d) evaluate the shape gradient $\nabla J_h(\Omega^{(k)}) = \nabla J(\Omega^{(k)}, \mathbf{y}_h^{(k)}, \mathbf{z}_h^{(k)})$ of the cost functional;
(e) update the shape of the domain and obtain $\Omega^{(k+1)}$,

until a suitable stopping criterion is satisfied; a possible choice is to require the difference between two subsequent values of the cost functional to be under a small, fixed tolerance $\tau > 0$. Concerning the shape update, let us recall that, thanks to the Hadamard's Structure Theorem (see, *e.g.*, [13]), the shape gradient $\nabla J$ can be expressed as

$$\nabla J = H(\Omega)|_{\Gamma_M} \, \mathbf{n}$$

where $\Gamma_M \subseteq \Gamma_b$ is the only boundary portion on which we can act during the optimization process. Thus, similarly to the *steepest descent method* for finite-dimensional optimization, we can in principle deform the boundary of $\Omega^{(k)}$ to obtain $\Omega^{(k+1)}$ as

$$\Omega^{(k+1)} = \mathbf{T}_k(\Omega^{(k)}) = (\mathbf{I} + \alpha_k \boldsymbol{\theta}_k)(\Omega^{(k)}), \qquad \text{where } \boldsymbol{\theta}_k = -H(\Omega^{(k)})\mathbf{n}^{(k)}, \tag{4.9}$$

where $\mathbf{n}^{(k)}$ denotes the unit outward normal on $\partial\Omega^{(k)}$ and $\alpha_k$ a suitable (small) step size; this techniques usually goes under the name of *local boundary variation* (LBV). The definition of the displacement $\boldsymbol{\theta}_k$ can be easily extended to the whole domain $\Omega^{(k)}$, through an harmonic extension (or Dirichlet-to-Neumann map) [1, 2] in order to prevent lack of regularity of the deformation map. To deal with the volume constraint in (2.12) we introduce a suitable Lagrange multiplier $l^{(k)} \in \mathbb{R}$, following the approach introduced in [2]. Hence, at the $k$th iteration, the descent direction in the gradient method is given by

$$J'(\Omega^{(k)})(\boldsymbol{\theta}_k) + l^{(k)}\, V'(\Omega^{(k)})(\boldsymbol{\theta}_k),$$

where $V'(\Omega)(\boldsymbol{\theta})$ is the shape derivative of the volume $|\Omega|$ of the generic domain $\Omega$, evaluated in the direction of $\boldsymbol{\theta}$. The Lagrange multiplier $l^{(k)}$ is selected by imposing the volume constraint (at least in the average sense) on the optimal domain, and it is updated according to the following rule:

$$l^{(k)} = \frac{l^{(k-1)} - \bar{l}^{(k-1)}}{2} + \epsilon(|\Omega^{(k-1)}| - \overline{V}) \qquad \text{with } \bar{l}^{(k-1)} = -\frac{\int_{\Gamma_M^{(k-1)}} H(\Omega)\mathrm{d}\sigma}{\int_{\Gamma_M^{(k-1)}} \mathrm{d}\sigma},$$

where $\overline{V}$ is the reference domain volume and $\epsilon > 0$ a chosen parameter.

For the case at hand, we exploit instead a *NURBS Free Form Deformation* (FFD) map [31, 46, 47] to handle domain deformations by dealing with a small number of *design variables*, instead than the whole set of nodes lying on the boundary to be deformed. Then, the deformation is extended to the whole domain through an interpolation with B-splines functions. The following subsection is devoted to the description of the NURBS-FFD map; the whole shape optimization procedure is sketched in Algorithm **3**, Appendix 6.

### 4.3. Free form deformation map based on NURBS

Deformation techniques based on FFD maps are often used in shape optimization problems for their low dimensionality: indeed, a FFD map yields a deformation for the whole domain by interpolating the displacement of a small set of control points. Such a map is defined on a *bounding box* (*e.g.*, a rectangle or a parallelepiped in two or three dimensions, respectively), including the shape being deformed; this also allows to solve shape optimization problems involving more complex figurations, too. In the last decades, many extensions of the FFD map originally introduced in [49] have been proposed; we focus on the the FFD map based on NURBS that combines the low dimensionality given by FFD with a major regularity and flexibility typical of the NURBS representation. See *e.g.* [36] for further details about the use of FFD maps in shape optimization.

The FFD map based on NURBS (Non-Uniform Rational B-Splines) is different from the classic one for the types of polynomials used in the deformation process (B-Splines instead of Bernstein polynomials) and for the chance to define a set of control points freely within the bounding box, rather than on a tensor lattice as in the classical FFD map. Besides the small dimension of the design variables set, FFD-based deformations allow to preserve the regularity of the domain boundary better than the LBV method. Our NURBS-FFD algorithm to handle shape deformations proceeds as follows:

(1) *initialization*: we first introduce an initial *bounding box* parametrized with suitable B-Splines. In particular, given a grid of *control points* $\{\mathbf{P}_{i,j}\}_{i=1,\dots,n\, j=1,\dots,m} \in \mathbb{R}^2$ and two *knot vectors* $\mathbf{U} \in \mathbb{R}^n$ and $\mathbf{V} \in \mathbb{R}^m$, it is possible to define a NURBS surface $\mathbf{S}(u, v)$ as follows:

$$\mathbf{S}(u, v) = \sum_{i=1}^{n} \sum_{j=1}^{m} N_{i,p}(u) N_{j,q}(v) \mathbf{P}_{i,j},$$

where $N_{i,p}(u)$, $N_{j,q}(v)$ represent the B-Spline bases[3] of degree $p$ (resp. $q$) related to the knot vector $\mathbf{U}$ (resp. $\mathbf{V}$), see *e.g.* [44] for further details. Furthermore, given the deformation $\mathbf{d}_{i,j}$ of the control point $\mathbf{P}_{i,j}$, we define the deformation of a generic point $\mathbf{p} = (\tilde{u}, \tilde{v}) \in \mathbf{S}$ as follows:

$$\mathbf{F}(\mathbf{p}) = \mathbf{p} + \sum_{i=1}^{n}\sum_{j=1}^{m} N_{i,p}(\tilde{u}) N_{j,q}(\tilde{v}) \mathbf{d}_{i,j}. \tag{4.10}$$

The nodes and the control points of the NURBS surface are such that (4.10) results in the identity map when zero displacement is imposed over the volume; see *e.g.* [46] for the detailed description of the strategy adopted to individuate the position of the nodes and the control points;

(2) *displacement definition*: we introduce a set of design variables $\{\mathbf{p}_s\}_{s=1,\dots,d}$, with $\mathbf{p}_s = (u_s, v_s)$, on which we define a desired deformation, by imposing that $\{\mathbf{p}_s\}_{s=1,\dots,d}$ are moved to $\{\mathbf{q}_s\}_{s=1,\dots,d}$ under the action of the map $\mathbf{F}$. Thus, we need to find a deformation expressed under the form (4.10), in order the Euclidean distance between $\mathbf{F}(\mathbf{p}_s)$ and $\mathbf{q}_s$ to be minimized. To this aim, we apply an iterative procedure in which the deformation of the point $\mathbf{p}_s$ at the iteration $t$ reads as

$$\mathbf{F}^{(t)}(\mathbf{p}_s) = \mathbf{F}^{(t-1)}(\mathbf{p}_s) + \sum_{i=1}^{n}\sum_{j=1}^{m} N_{i,p}(u_s) N_{j,q}(v_s)\, \mathbf{d}_{i,j}^{(t)}.$$

To define a FFD map it is sufficient to describe its effects over the control points used to parametrize the NURBS initial volume; therefore, the minimization problem above is equivalent to find the vector $\mathbf{d}^{(t)}$ of control points displacements by solving the following least-squares problem (see [47] for further details about the computational procedure):

$$\mathbf{d}^{(t)} = \underset{\mathbf{x}\in\mathbb{R}^{n\times m}}{\operatorname{argmin}} \sum_{s=1}^{d} \left\| \sum_{i=1}^{n}\sum_{j=1}^{m} (N_{i,p}(u_s) N_{j,q}(v_s)\, \mathbf{x}_{i,j}) - (\mathbf{q}_s - \mathbf{F}^{(t-1)}(\mathbf{p}_s)) \right\|_2^2;$$

(3) *deformation*: by using the position $\mathbf{d}_{i,j}$ of the displaced control points $\mathbf{P}_{i,j}$ found at the previous step, we can finally apply the evaluate the action of the map $\mathbf{F}(\cdot)$ defined in (4.10) on each node of the computational mesh $\Omega$, and therefore obtain the deformed domain $\mathbf{F}(\Omega)$.

## 5. Numerical results

We now show some numerical results obtained on simplified two-dimensional geometries. The goal of the proposed test cases is threefold, since we want *(i)* to verify the feasibility of the proposed algorithm; *(ii)* to compare the optimal shape of a simple structure in presence of FSI with the results obtained for a rigid geometry, showing that we recover the results of the rigid case as the stiffness of the structure increases; *(iii)* to show the effectiveness of the adjoint-based procedure in the optimization framework.

Let us consider the two-dimensional reference domain $\Omega_0$ shown in Figure 1, discretized with a computational mesh made by 2313 nodes, as fluid domain, and the one-dimensional domain $\Gamma_0 = (0, L)$ approximated with 240

[3]The basis $N$ of grade 0 is defined as follows:

$$N_{i,0}(u) = \begin{cases} 1 \text{ if } u_i \le u \le u_{i+1} \\ 0 \text{ otherwise,} \end{cases}$$

where $u_i$ are the knots in the vector $\mathbf{U}$. The basis $N_{i,p}$ are defined recursively through the Cox-de Boor formula as

$$N_{i,p}(u) = \frac{u - u_i}{u_{i+p} - u_i} N_{i,p-1}(u) + \frac{u_{i+p+1} - u}{u_{i+p+1} - u_{i+1}} N_{i+1,p-1}(u).$$

TABLE 1. Physical and geometrical parameters in the FSI problem.

| | | | |
|---|---|---|---|
| Geometrical parameters | | | |
| Domain radius | $R$ | 0.5 | cm |
| Domain length | $L$ | 6 | cm |
| Fluid parameters | | | |
| Density | $\rho_F$ | 1 | $g\,\mathrm{cm}^{-3}$ |
| Viscosity | $\mu_F$ | 0.63 | $P$ |
| Structural parameters | | | |
| Density | $\rho_S$ | 1.1 | $\mathrm{g\,cm}^{-3}$ |
| Thickness | $h_S$ | 0.1 | cm |
| Viscosity | $\mu_S$ | $2.5 \times 10^4$ | P |
| Coefficient | $\beta$ | $4 \times 10^5$ | $\mathrm{dyn\,cm}^{-3}$ |
| Young modulus | $E$ | $0.75 \times 10^6$ | $\mathrm{dyn\,cm}^{-2}$ |
| Poisson coefficient | $\nu$ | 0.5 | – |

nodes. The portion $\Gamma_M \subset \Gamma_0$ is the portion of the boundary on which we can act for the sake of optimization. Concerning the time discretization, we subdivide the time interval $(0, 0.03s)$ with a time step $\Delta t = 0.001\ s$. To deform the fluid reference domain we use a NURBS-FFD map with an initial FFD volume described with $40 \times 10$ control points and B-splines with order 2 in each dimension $x_1, x_2$. Regarding the finite element discretization, we approximate the velocity and the pressure of the fluid sub-problem by means of quadratic and linear (Lagrangian) basis functions, respectively, in order to ensure the discrete inf-sup stability of the Stokes problem; the displacement of the solid structure is approximated through quadratic (Lagrangian) basis functions. To define the deformation, we introduce 100 design variables lying on the boundary $\Gamma_M$ of the reference domain, which can be displaced along the vertical direction. Finally, the relaxation parameters $\gamma$ in (4.3) and $\omega$ in (4.6) are set equal to 0.75, according to an heuristic *trial-and-error* procedure inspired from the results presented in [9]. Although in a much more simplified framework dealing with inviscid fluids interacting with a Koiter model like the one at hand, in [9] it is shown that the Dirichlet−Neumann coupling on an FSI problem close to our state problem indeed converges for values of $\gamma < \bar{\gamma} = 0.85$. To reach convergence, the FSI solver requires about $3 \div 5$ iterations (see Algorithm (**1**)), also because the structure is undergoing small deformations in the considered test cases.

Geometrical and physical parameters (for both the fluid and the structure) are chosen according to typical values of fluid and structural properties in haemodynamical applications – such has blood density and viscosity, arterial wall Young modulus, *etc.* – according to the motivation that has inspired this work; their values are listed in Table 1. Regarding the inflow boundary condition of the fluid problem, given a maximum velocity $u_{\max} = 75$ cm/s the inlet velocity profile $\mathbf{u}_{\text{in}}$ takes the form

$$\mathbf{u}_{\text{in}} = (u_{\text{in}}, 0)^T \qquad \text{with } u_{\text{in}} = \begin{cases} \dfrac{4u_{\max}}{R} y \left(1 - \dfrac{y}{R}\right) & \text{for} \quad t \leq 0.01\ s \\ 0 & \text{for} \quad t > 0.01\ s, \end{cases} \tag{5.1}$$

being $R = 0.5\,\mathrm{cm}$ the length of the inlet $\Gamma_{\text{in}}$.

### 5.1. Test case 1

As first test case, we compare the optimal shapes obtained with *(i)* the proposed procedure based on the NURBS-FFD map and (ii) the LBV method. Although the value of the cost functional at the optimum is indeed very similar – $J(\hat{\Omega}_{FFD}) = 44.953$ in the NURBS-FFD case vs. $J(\hat{\Omega}_{LBV}) = 44.956$ in LBV case, starting from an initial shape for which $J(\Omega_0) = 46.364$ – the optimal domain obtained with the two methods are quite different. As shown in Figure 3, the boundary of the shape deformed by the NURBS-FFD map results more regular than the one obtained with the LBV method, although the number of design variables in this latter case

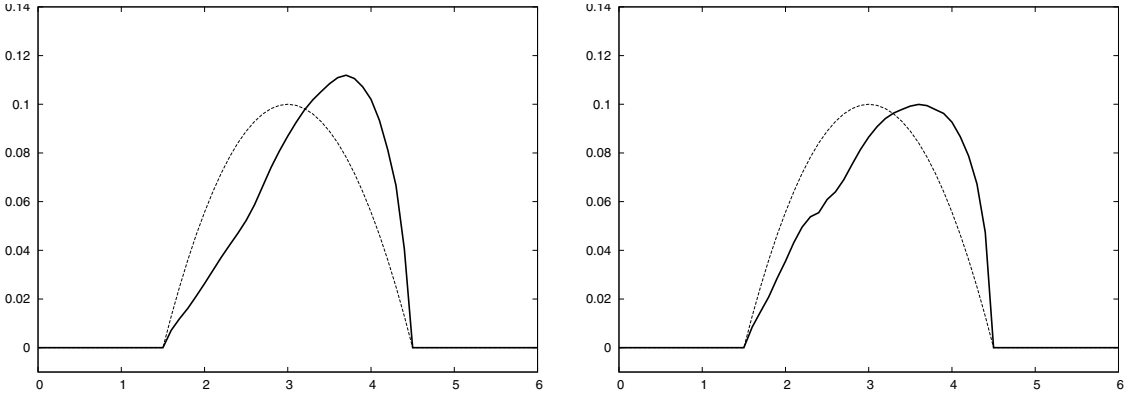


(A) NURBS-FFD map (B) LBV method

FIGURE 3. Inferior boundary of the optimal shape, varying the domain updating method.

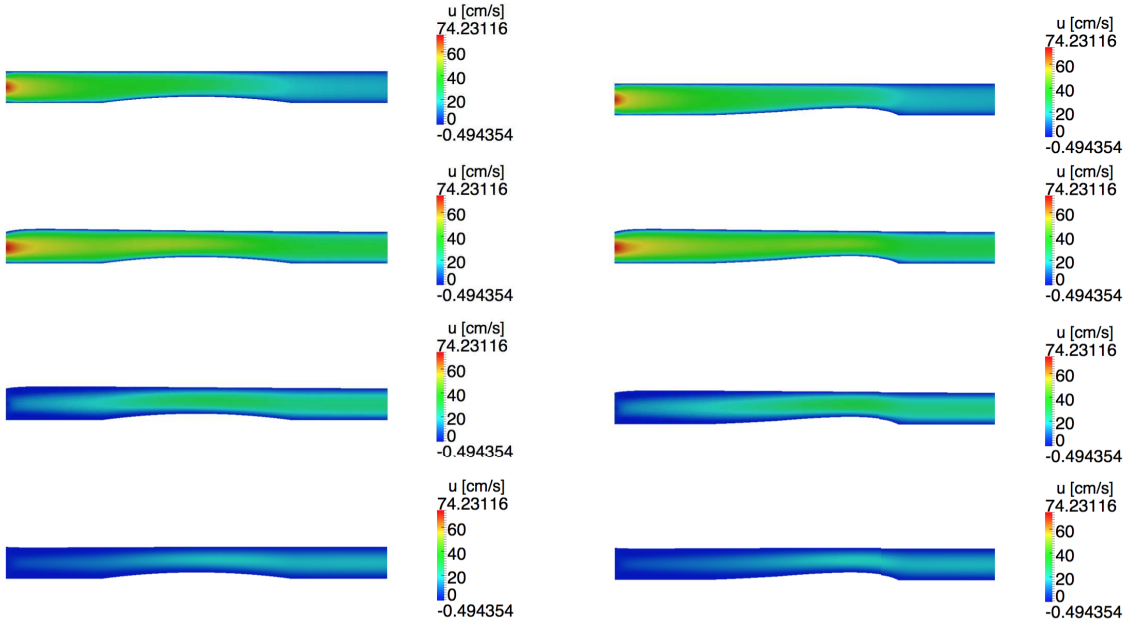


FIGURE 4. Fluid velocity at different time-steps (*from top to bottom*: $t = 0.005, 0.01, 0.015, 0.02$) in the reference (*left*) and the optimal (*right*) domain.

is twice as large as the one in the former. Moreover, the algorithm based on the NURBS-FFD map converges in 16 iterations, whereas the one based on the LBV method takes 30 iterations to reach the optimum. For these reasons, in the following test case we rely on the NURBS-FFD map in order to handle domain deformations during the optimization process. In Figures 4 and 5 the fluid velocity and pressure at different time-steps, in the reference domain $\Omega_0$ and in the optimal configuration, are shown.

## 5.2. Test case 2

In the second test case, starting from the initial configuration already considered in test case 1, we compare the optimal shape $\hat{\Omega}_{FSI}$ obtained in the case of a deformable structure – whose wall indeed moves under the

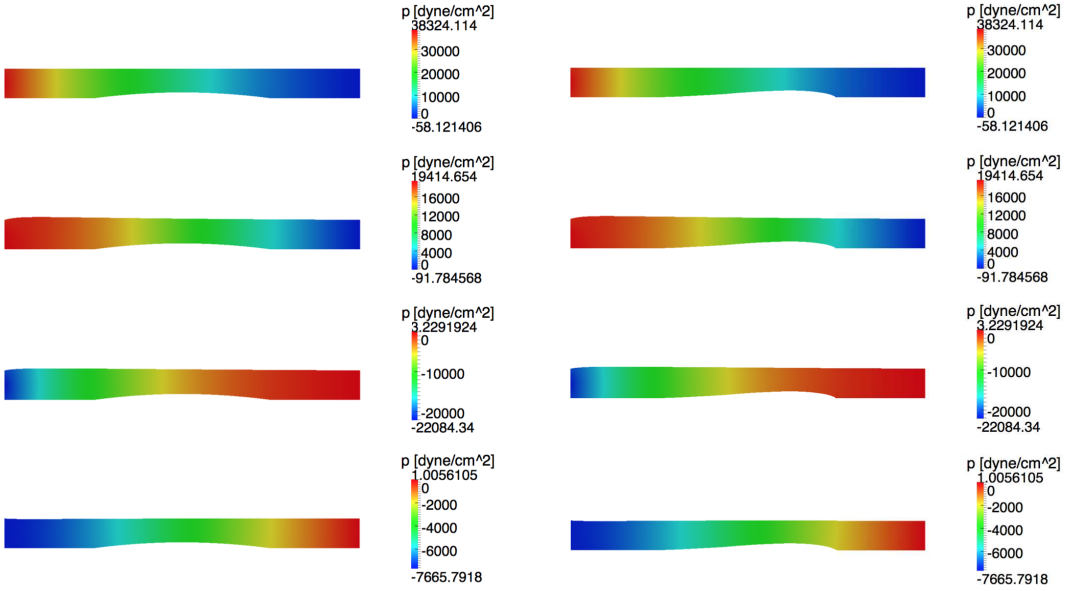


FIGURE 5. Fluid pressure at different time-steps (*from top to bottom*: $t = 0.005, 0.01, 0.015, 0.02$) in the reference (*left*) and the optimal (*right*) domain.

effect of the fluid flow – with the one, $\hat{\Omega}_S$, obtained by considering a rigid structure; in this latter case, we set the Dirichlet condition $\mathbf{u} = \mathbf{0}$ on the interface $\Gamma(t)$ in the fluid equations. In Figure 6, the optimal shapes obtained in these two scenarios are shown; even if we are dealing with a linear Stokes flow, the difference between the optimal shapes obtained in these two cases is not negligible. By evaluating the solution to the FSI problem in the two optimal configurations, we obtain that $44.956 = J(\hat{\Omega}_{FSI}) \leq J(\hat{\Omega}_S) = 44.988$. From a computational point of view, dealing with a deformable structure entails a CPU cost which is more than 50% higher with respect to the case of a rigid structure: each iteration of the optimization procedure takes about 120 $s$ in the rigid case and about 210 $s$ in the FSI case with a Intel Premium P6100 processor with 2.00 GHz of clock speed and 4GB RAM. Furthermore, we can show (see Fig. 7) that the optimal shape obtained in the rigid case can be obtained as the limit of the optimal shapes in presence of FSI, when increasing the stiffness of the wall. In fact, the higher the value of the Young modulus $E$, the closer the optimal shape to the one obtained in the case of a rigid wall.

### 5.3. Test case 3

As seen in Section 3.2, dealing with the adjoint problem for the structure (3.16) is a difficult matter, for the sake of both its derivation and its numerical approximation. Note also that the gradient of the the cost functional reported in equation (3.21) does not involve the solid adjoint variable – but also the fluid adjoint variable, which is nevertheless coupled to the former. For this reason, we consider an *adjoint-free* method, in which the solid adjoint problem is not considered, and the FSI adjoint solution is approximated by the fluid adjoint solution. Hence, we compare the optimal shape obtained by relying on the solution to an adjoint problem for both the fluid and the structure, with the one obtained by considering only the fluid adjoint problem. In particular, also in this case we rely on the procedure of Sect. 4.2, but evaluating at step (c) only the solution of the fluid adjoint problem, that is, $\mathbf{z}_h^{(k)} = (\mathbf{v}_h^{(k)}, q_h^{(k)})$. We report in Figure 8 the results obtained with an *adjoint-free* method, in which the full FSI state problem (2.2), (2.7), (2.8) is solved, whereas the only fluid adjoint problem (3.5) is considered: the optimal configurations in these two cases are clearly different, thus

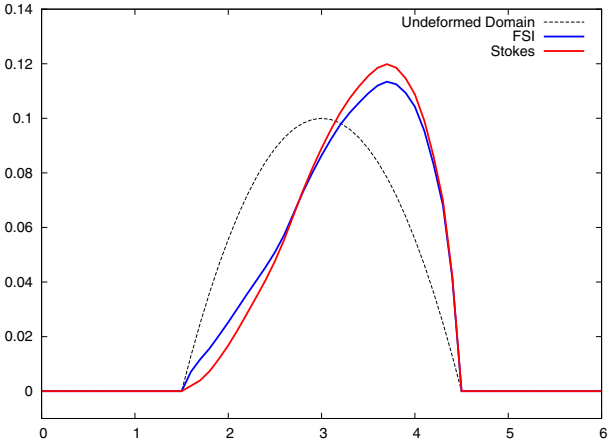


FIGURE 6. Optimal shapes obtained in the FSI case (in blue) and the case of a rigid structure (in red).

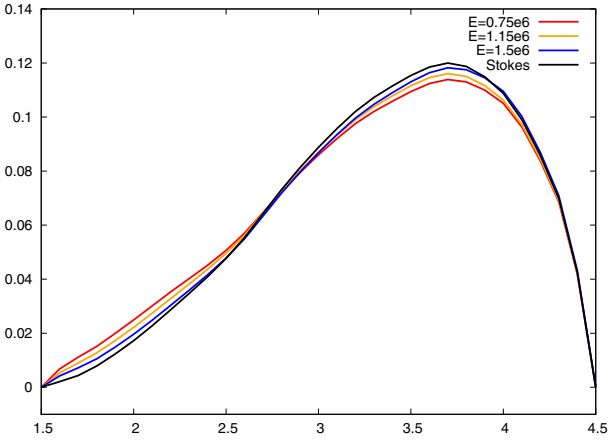


FIGURE 7. Optimal shape obtained for different values of the Young Modulus $E$.

indicating that each optimality condition is indeed important; the adjoint-based procedure thus cannot avoid to include the structural adjoint problem.

### 5.4. Test case 4

In this last test case, we show the results obtained by considering as initial configuration in the optimization process the one described in Figure 9, that is, by assuming (unlike the previous tests) that the whole bottom boundary domain is subject to design. In Figure 10 we report the optimal shapes obtained by admitting that the whole inferior boundary can be optimized, either in the FSI case or by considering a rigid wall. Note that for $x \in (1.5, 4.5)$ the optimal profile resembles the one shown in Figure (6), where only the portion of the lower boundary with $x \in (1.5, 4.5)$ was optimized. Close to those points where the reference domain is not $C^1$, also the optimal shape shows less regularity; such a behavior is a well-known problem (see *e.g.* [44]) in the application of the NURBS-FFD map *e.g.* for the sake of optimal shape design. Nevertheless, the enlargement of the sections of the optimal domain close to the inlet boundary can be found in similar results obtained when dealing with shape optimization problems of Stokes flows with rigid domains, see *e.g.* [21]. Regarding the decrease of the cost

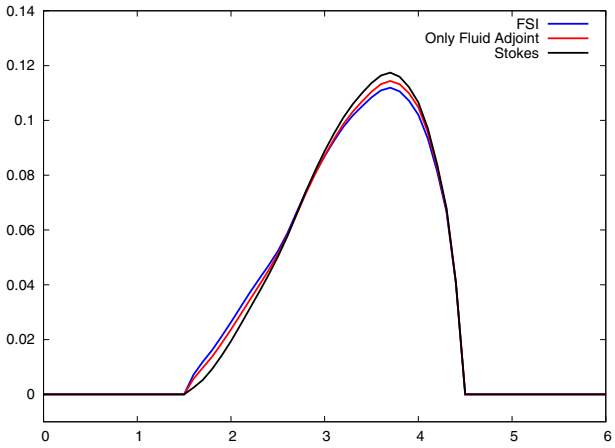


FIGURE 8. Optimal shape obtained with the *adjoint-free* method (in red), the *adjoint-based* method involving the solution to the structural adjoint problem (in blue) and assuming that the structure is rigid (in black).

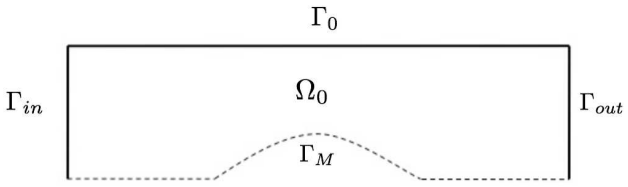


FIGURE 9. Test case 4. Reference configuration used as starting point of the optimization process.

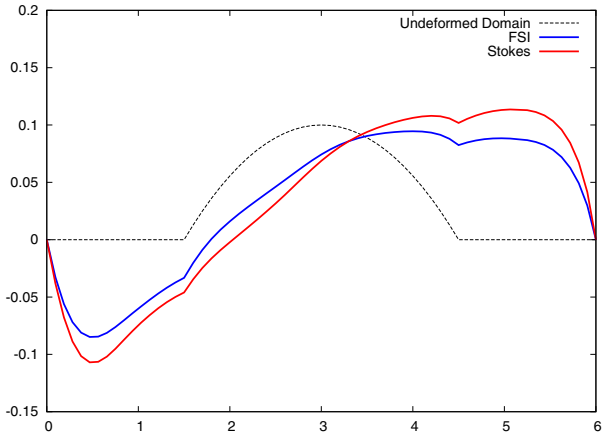


FIGURE 10. Optimal shapes (FSI case in blue, rigid case in red) obtained by considering as initial configuration the one in Figure 1, with the whole bottom boundary $\Gamma_0 \cup \Gamma_M$ subject to design.

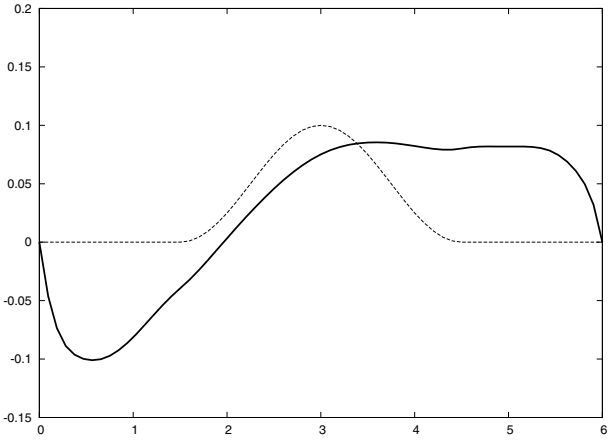


FIGURE 11. Optimal shape (FSI case) obtained by considering as initial configuration a reference domain with bottom boundary (dashed) globally $C^1$ and entirely subject to design.

functional, a better result is obtained (as expected) when allowing the whole lower boundary to be deformed. In the FSI case, the cost functional evaluated in the optimal shape is equal to $J(\hat{\Omega}) = 42.228$, a much smaller value than the one (44.956) obtained when only the central portion of $\Gamma_M$ could be deformed.

Finally, in order to show that the lack of regularity was induced by the local $C^0$ regularity of the reference configuration, we investigate the regularity of an optimal configuration obtained by considering a reference domain with a $C^1$ lower boundary. By solving the shape optimization problem in the FSI case and imposing that the whole lower boundary can be deformed, we obtain the optimal shape reported in Figure 11, which preserves the regularity of the initial one; the cost functional in this case decreases from the initial value $J(\Omega_0) = 42.45$ to the optimal value $J(\hat{\Omega}) = 40.92$.

## 6. Conclusions

In this paper we have developed an adjoint-based method for the numerical approximation of shape optimization problems in presence of fluid-structure interaction. In particular, we have characterized the optimal solution as the saddle point of a suitable Lagrangian functional, showing how to derive a system of first-order necessary optimality conditions, where the most difficult task is the recovery of a suitable solid adjoint problem for the structural subproblem. The procedure described to address the difficulties arising from the FSI coupling is fairly general, although we have focused on unsteady Stokes flows for the sake of simplicity.

Based on this optimality system, we have implemented a numerical solver for the shape optimization problem, involving a Dirichlet−Neumann approach for solving the state FSI problem. An additional difficulty tackled in this work is given by the numerical solution to the adjoint FSI problem, for which only few results are indeed available in literature. We have implemented an efficient solver of the adjoint FSI problem taking advantage of the numerical scheme used for the state FSI problem. Finally, we have exploited a steepest descent-like method for the sake of numerical optimization, where the optimal structural configuration is obtained by taking advantage, at each step, of the shape gradient of the cost functional. To deal with domain deformations efficiently, we have implemented an algorithm based on the NURBS Free Form Deformation map, which ensures higher boundary regularity of each deformed domain, as well as a faster convergence to the optimum than the local boundary variation method.

We have assessed the feasibility of the proposed procedure by performing different test cases varying the elastic parameter of the structure, showing that the stiffer the material, the closer the optimal shape to the one

obtained by considering a rigid structure. Finally, we showed the importance of the solution to the structural adjoint problem, by comparing our results obtained with those obtained through an *adjoint-free* method.

## Appendix A. Proof of Lemma 3.4

In this Appendix we prove Lemma 3.4, yielding the expression of the derivative

$$\frac{\mathrm{d}}{\mathrm{d}\rho}\left(\int_0^T\int_{\Gamma_\rho(t)}\phi(\rho)\mathrm{d}\sigma\,\mathrm{d}t\right)\Bigg|_{\rho=0} \tag{A.1}$$

being

$$\phi(\rho)=-\rho_F(\mathbf{u}_\rho\cdot\mathbf{v}_\rho)\left(\frac{\partial(\eta+\rho\delta\eta)}{\partial t}\circ(\eta+\rho\delta\eta)^{-1}\mathbf{e}_2\right)\cdot\mathbf{n}^\rho. \tag{A.2}$$

We recall some results (see, *e.g.*, [38] for their proof) useful to evaluate the expression above:

**Lemma A.1.** *Let $\Omega_0\subset\mathbb{R}^d$ be a fixed domain and $\Gamma_0$ a subset of its boundary $\partial\Omega_0$. Let us denote*

$$\Gamma_\rho=\{\mathbf{x}\in\mathbb{R}^d\ :\ \mathbf{x}=(\mathbf{I}+\rho\boldsymbol{\gamma})\mathbf{x}_0,\ \mathbf{x}_0\in\Gamma_0\},$$

*where $\boldsymbol{\gamma}\in W^{1,\infty}(\mathbb{R}^n;\mathbb{R}^n)$ and let $\mathbf{E}(\rho)$ be a field vector defined on $D$ with $D\supset(\Gamma_0\cup\Gamma_\rho)$, then the following identity holds*:

$$\frac{\mathrm{d}}{\mathrm{d}\rho}\left(\int_{\Gamma_\rho}\mathbf{E}(\rho)\cdot\mathbf{n}^\rho\,\mathrm{d}\sigma\right)\Bigg|_{\rho=0}=\int_\Gamma\left(\frac{\partial\mathbf{E}}{\partial\rho}\Big|_{\rho=0}\cdot\mathbf{n}+\mathrm{div}\mathbf{E}\,(\boldsymbol{\gamma}\cdot\mathbf{n})\right)\mathrm{d}t.$$

*being $\mathbf{n}^\rho$ the unit outward normal on $\Gamma_\rho$.*

**Lemma A.2.** *Let $\eta\in H^2(0,T;H^2(\Gamma(t)))$, then:*

$$\mathbf{W}_0:=\frac{\mathrm{d}}{\mathrm{d}\rho}\left(\frac{\partial(\eta+\rho\delta\eta)}{\partial t}\circ(\eta+\rho\delta\eta)^{-1}\right)\Bigg|_{\rho=0}\mathbf{e}_2=\frac{\partial(\delta\eta\circ\eta^{-1})}{\partial t}\mathbf{e}_2-\nabla\left(\left(\frac{\partial\eta}{\partial t}\circ\eta^{-1}\right)\mathbf{e}_2\right)\gamma. \tag{A.3}$$

**Lemma A.3.** *Let $\mathbf{F}$ be a vector field defined on the domain $D$ such as $\Omega(t)\subset D\ \forall t\geq 0$; then the following idenitity holds:*

$$\int_0^T\int_{\Gamma(t)}\frac{\partial(\delta\eta\circ\eta^{-1})}{\partial t}\mathbf{F}\cdot\mathbf{e}_2\mathrm{d}\sigma\mathrm{d}t=\int_0^T\int_{\Gamma(t)}\left[-\frac{\partial\mathbf{F}}{\partial t}-(\mathrm{div}_{\Gamma(t)}\mathbf{u}_s)\,\mathbf{F}-\nabla\mathbf{F}\,\mathbf{u}_S\right]\cdot\boldsymbol{\gamma}\mathrm{d}\sigma\mathrm{d}t+\left[\int_{\Gamma(t)}\mathbf{F}\,\boldsymbol{\gamma}\mathrm{d}\sigma\right]_0^T. \tag{A.4}$$

We are now ready to prove Lemma 3.4.

*Proof.* We first point out that the term $\phi(\rho)$ can be written in the form $\phi(\rho) = \mathbf{E}(\rho) \cdot \mathbf{n}^\rho$, where $\mathbf{E}(\rho)$ is defined as follows:

$$\mathbf{E}(\rho) = -\rho_F(\mathbf{u}_\rho \cdot \mathbf{v}_\rho) \left( \frac{\partial(\eta + \rho\delta\eta)}{\partial t} \circ (\eta + \rho\delta\eta)^{-1} \right) \mathbf{e}_2.$$

Thus, by using the Lemma A.1 and the Lemma A.2, the derivative (A.1) reads:

$$\begin{aligned} \frac{\mathrm{d}}{\mathrm{d}\rho} \left( \int_0^T \int_{\Gamma_\rho(t)} \phi(\rho) \mathrm{d}\sigma \mathrm{d}t \right) \Bigg|_{\rho=0} &= -\rho_F \int_0^T \int_{\Gamma(t)} (\mathbf{u} \cdot \mathbf{v})(\mathbf{W}_0 \cdot \mathbf{n}) \mathrm{d}\sigma \, \mathrm{d}t \\ &+ \rho_F \int_0^T \int_{\Gamma(t)} \left[ (\nabla \mathbf{u}\, \boldsymbol{\gamma}) \cdot \mathbf{v} + (\nabla \mathbf{v}\, \boldsymbol{\gamma}) \cdot \mathbf{u} \right] (\mathbf{u}_S \cdot \mathbf{n}) \mathrm{d}\sigma \, \mathrm{d}t \\ &- \rho_F \int_0^T \int_{\Gamma(t)} \left[ \nabla(\mathbf{u} \cdot \mathbf{v}) \cdot \mathbf{u}_S + (\mathbf{u} \cdot \mathbf{v}) \operatorname{div} \mathbf{u}_S \right] (\boldsymbol{\gamma} \cdot \mathbf{n}) \mathrm{d}\sigma \, \mathrm{d}t. \end{aligned}$$

The expression above can be simplified again by recalling the definition of the term $\mathbf{W}_0$ and by suitably erasing the time derivative of the variation $\delta\eta$. Thus, by setting $\mathbf{F} = \rho_f(\mathbf{u} \cdot \mathbf{v})\mathbf{n}$ in Lemma A.3, we have:

$$\begin{aligned} \frac{\mathrm{d}}{\mathrm{d}\rho} \left( \int_0^T \int_{\Gamma_\rho(t)} \phi(\rho) \mathrm{d}\sigma \mathrm{d}t \right) \Bigg|_{\rho=0} &= \rho_F \int_0^T \int_{\Gamma(t)} \left( \frac{\partial \mathbf{u}}{\partial t} \cdot \mathbf{v} + \frac{\partial \mathbf{v}}{\partial t} \cdot \mathbf{u} \right) (\boldsymbol{\gamma} \cdot \mathbf{n}) \mathrm{d}\sigma \, \mathrm{d}t \\ &+ \rho_F \int_0^T \int_{\Gamma(t)} \left[ (\nabla((\mathbf{u} \cdot \mathbf{v})\mathbf{n})\, \mathbf{u}_S) \cdot \boldsymbol{\gamma} - \nabla(\mathbf{u} \cdot \mathbf{v})(\boldsymbol{\gamma} \cdot \mathbf{n}) \right] \mathrm{d}\sigma \, \mathrm{d}t \\ &- \rho_F \int_{\Gamma(T)} (\mathbf{u} \cdot \mathbf{v})(T)(\boldsymbol{\gamma} \cdot \mathbf{n}) \mathrm{d}\sigma + \rho_F \int_{\Gamma_0} (\mathbf{u}_0 \cdot \mathbf{v}(0))(\boldsymbol{\gamma} \cdot \mathbf{n}) \mathrm{d}\sigma \\ &+ \rho_F \int_0^T \int_{\Gamma(t)} \left[ (\nabla \mathbf{u}\, \boldsymbol{\gamma}) \cdot \mathbf{v} + (\nabla \mathbf{v}\, \boldsymbol{\gamma}) \cdot \mathbf{u} \right] (\mathbf{u}_S \cdot \mathbf{n}) \mathrm{d}\sigma \, \mathrm{d}t. \end{aligned}$$

We now seek to semplify the term $(\nabla((\mathbf{u} \cdot \mathbf{v})\mathbf{n})\, \mathbf{u}_S) \cdot \boldsymbol{\gamma} - \nabla(\mathbf{u} \cdot \mathbf{v})(\boldsymbol{\gamma} \cdot \mathbf{n})$. For the ease of the reader, let us denote $f = (\mathbf{u} \cdot \mathbf{v})$, $\mathbf{u}_S = (0, u_S)^T$ and $\mathbf{n} = (n_1, n_2)^T$; then, the following identities hold:

$$\begin{aligned} \rho_F(\nabla f \cdot \mathbf{u}_S)(\boldsymbol{\gamma} \cdot \mathbf{n}) &= \rho_F \frac{\partial f}{\partial y} \delta\eta \, u_S \, n_2, \\ \rho_F(\nabla(f\,\mathbf{n})\, \mathbf{u}_S) \cdot \boldsymbol{\gamma} &= \rho_F \frac{\partial (f\, n_2)}{\partial y} u_S \, \delta\eta = \rho_F \left( \frac{\partial f}{\partial y} n_2 + \frac{\partial n_2}{\partial y} f \right) u_S \, \delta\eta, \end{aligned}$$

We now subtract the two equations above and we recall that the tangential gradient of the unit normal $\mathbf{n}$ is given by

$$\nabla_{\Gamma(t)} \mathbf{n} = \nabla \mathbf{n} - \mathbf{N},$$

being $\mathbf{N}$ the matrix defined as $N_{ij} = n_i \delta_{ij}$. Thus, we have:

$$(\nabla((\mathbf{u} \cdot \mathbf{v})\mathbf{n})\, \mathbf{u}_S) \cdot \boldsymbol{\gamma} - \nabla(\mathbf{u} \cdot \mathbf{v})(\boldsymbol{\gamma} \cdot \mathbf{n}) = \rho_F(\mathbf{u} \cdot \mathbf{v})((\nabla_{\Gamma(t)} \mathbf{n} + \mathbf{N})\, \mathbf{u}_S) \cdot \boldsymbol{\gamma},$$

which concludes the proof of the lemma. □

## Appendix B. Proof of Lemma 3.5

The proof of Lemma 3.5 is based on the so-called *shape derivative kernel identity* (see, *e.g.*., Lem. 8.14, [38]), which for the case at hand reads as follows:

**Lemma B.1.** *Let* $(\mathbf{u}, p, \mathbf{v}, q, \boldsymbol{\lambda}_F) \in V_F(\Omega) \times Q_F(\Omega) \times V_0(\Omega) \times Q_F(\Omega) \times L^2(0,T; H^1(\mathbb{R}^2))$ *be a saddle point of the Lagrangian functional* $\mathcal{L}$ *defined in* (3.3)*. Then the following identity holds:*

$$
\begin{aligned}
&\alpha \int_0^T \int_{\Omega(t)} \nabla \mathbf{u} : \nabla(\nabla \mathbf{u}\, \boldsymbol{\gamma})\, \mathrm{d}\mathbf{x}\, \mathrm{d}t + \rho_F \int_0^T \int_{\Omega(t)} \left( (\nabla \mathbf{u}\, \boldsymbol{\gamma}) \cdot \frac{\partial \mathbf{v}}{\partial t} + \mathbf{u} \cdot \frac{\partial (\nabla \mathbf{v}\, \boldsymbol{\gamma})}{\partial t} \right) \mathrm{d}\mathbf{x}\, \mathrm{d}t \\
&+ \int_0^T \int_{\Omega(t)} \left( p \operatorname{div}(\nabla \mathbf{v}\, \boldsymbol{\gamma}) + q \operatorname{div}(\nabla \mathbf{u}\, \boldsymbol{\gamma}) \right) \mathrm{d}\mathbf{x}\, \mathrm{d}t - \mu_F \int_0^T \int_{\Omega(t)} \left( \nabla \mathbf{u} : \nabla(\nabla \mathbf{v}\, \boldsymbol{\gamma}) + \nabla(\nabla \mathbf{u}\, \boldsymbol{\gamma}) : \nabla \mathbf{v} \right) \mathrm{d}\mathbf{x}\, \mathrm{d}t \\
&- \rho_F \int_{\Omega(T)} \left( (\nabla \mathbf{u}\, \boldsymbol{\gamma}) \cdot \mathbf{v} + \mathbf{u} \cdot (\nabla \mathbf{v}\, \boldsymbol{\gamma}) \right)(T)\, \mathrm{d}\mathbf{x} + \rho_F \int_{\Omega_0} \mathbf{u}_0 \cdot (\nabla \mathbf{v}(0)\, \boldsymbol{\gamma})\, \mathrm{d}\mathbf{x} \\
&+ \rho_F \int_0^T \int_{\Gamma(t)} (\mathbf{u}_S \cdot \mathbf{n}) \left( \mathbf{u} \cdot (\nabla \mathbf{v}\, \boldsymbol{\gamma}) + (\nabla \mathbf{u}\, \boldsymbol{\gamma}) \cdot \mathbf{v} \right) \mathrm{d}\sigma\, \mathrm{d}t \\
&+ \int_0^T \int_{\Gamma_D} \boldsymbol{\lambda}_F \cdot (\nabla \mathbf{u}\, \boldsymbol{\gamma}) + \int_0^T \int_{\Gamma(t)} (\boldsymbol{\sigma}^F(\mathbf{u}, p)\, \mathbf{n}) \cdot (\nabla \mathbf{v}\, \boldsymbol{\gamma}) \mathrm{d}\sigma\, \mathrm{d}t \\
&+ \int_0^T \int_{\Omega(t)} \left( (\nabla p \cdot \boldsymbol{\gamma}) \operatorname{div} \mathbf{v} + (\nabla q \cdot \boldsymbol{\gamma}) \operatorname{div} \mathbf{u} \right) \mathrm{d}\mathbf{x}\, \mathrm{d}t + \int_0^T \int_{\Gamma_D} (\nabla \boldsymbol{\lambda}_F\, \boldsymbol{\gamma}) \cdot (\mathbf{u} - \mathbf{u_D}) \mathrm{d}\sigma\, \mathrm{d}t = 0.
\end{aligned}
\tag{B.1}
$$

*Proof of Lemma B.1.* Let us define a Lagrangian functional $\mathcal{L}^d$ as we did for the Lagrangian functional $\mathcal{L}$ in (3.3), except for the fact that in $\mathcal{L}^d$ we consider test functions $(\mathbf{v}, \psi) \in V_0(\Omega) \times V_S$ and therefore discontinuous on $\Gamma(t)$, note that in $\mathcal{L}$ test functions $(\mathbf{v}, \psi) \in S(\Omega)$ are chosen to be continuous on the interface $\Gamma(t)$. Hence, the Lagrangian functional $\mathcal{L}^d$ assumes the following form:

$$
\mathcal{L}^d(\mathbf{u}, \eta, p; \mathbf{v}, \psi, q; \Omega) = \mathcal{L}(\mathbf{u}, \eta, p; \mathbf{v}, \psi, q; \Omega) + \int_0^T \int_{\Gamma(t)} (\boldsymbol{\sigma}^F(\mathbf{u}, p)\, \mathbf{n}) \cdot (\mathbf{v} - \psi \circ \eta^{-1} \mathbf{e}_2)\, \mathrm{d}\sigma \mathrm{d}t,
$$

where $\mathcal{L}$ is the Lagrangian functional defined in (3.3). Since by assumption $(\mathbf{u}, p, \mathbf{v}, q)$ is a saddle point of the Lagrangian functional $\mathcal{L}$, the following identity yields:

$$
\left\langle \frac{\partial \mathcal{L}^d}{\partial(\mathbf{u}, p, \mathbf{v}, q, \boldsymbol{\lambda}_F)}, (\delta\mathbf{u}, \delta p, \delta\mathbf{v}, \delta q, \delta\boldsymbol{\lambda}_F) \right\rangle = 0. \tag{B.2}
$$

Since (B.2) is fulfilled for any $(\delta\mathbf{u}, \delta p, \delta\mathbf{v}, \delta q\, \delta\boldsymbol{\lambda}_F) \in V_F(\Omega) \times Q_F(\Omega) \times V_0(\Omega) \times Q_F(\Omega) \times L^2(0,T; H^1(\mathbb{R}^2))$, we can select the following perturbations:

$$
\begin{aligned}
\delta\mathbf{u} &= \nabla \mathbf{u}\, \boldsymbol{\gamma}, & \delta\mathbf{v} &= \nabla \mathbf{v}\, \boldsymbol{\gamma}, \\
\delta p &= \nabla p \cdot \boldsymbol{\gamma}, & \delta q &= \nabla q \cdot \boldsymbol{\gamma}, \\
\delta\boldsymbol{\lambda}_F &= \nabla \boldsymbol{\lambda}_F\, \boldsymbol{\gamma}\,.
\end{aligned}
\tag{B.3}
$$

Hence, computing the derivative (B.2) of the Lagrangian functional $\mathcal{L}^d$ in the direction (B.3), and exploiting the continuity of the test functions enforced through the choice of the functional space $S(\Omega)$, we obtain the *shape derivative kernel identity* (B.1). This concludes the proof of Lemma B.1. □

Lemma B.1 allows to prove Lemma 3.5. As a matter of fact, by summing up the expression of the functional $A_\Omega$ given in (3.14) and the *shape derivative kernel identity* stated in (B.1), we obtain the following identity:

$$
A_\Omega = \int_0^T \int_{\Gamma(t)} (\rho_F(\mathbf{u}_S \cdot \mathbf{n})(\mathbf{u} \cdot (\nabla \mathbf{v}\, \boldsymbol{\gamma}) + (\nabla \mathbf{u}\, \boldsymbol{\gamma}) \cdot \mathbf{v})\, \mathrm{d}\sigma\, \mathrm{d}t + \int_0^T \int_{\Gamma(t)} (\boldsymbol{\sigma}^F(\mathbf{u}, p)\, \mathbf{n}) \cdot (\nabla \mathbf{v}\, \boldsymbol{\gamma})\, \mathrm{d}\sigma\, \mathrm{d}t,
$$

which indeed proves Lemma 3.5.

## Appendix C. Algebraic formulation of the Galerkin problem

The algebraic formulation of the Galerkin approximation of the fluid sub-problem (4.7) and the solid sub-problem (4.8) in the state equation of the FSI process is briefly sketched in this Appendix. Firstly, let us denote by $\{\boldsymbol{\varphi}_j^F\}_{j=1}^{N_F}$, $\{\phi_j\}_{j=1}^{N_Q}$, $\{\varphi_j^S\}_{j=1}^{N_S}$ the Lagrangian bases of the spaces $V_h^{F,n}, Q_h^n$ and $V_h^S$, respectively, and express the spatial approximation of $\mathbf{u}_h, p_h, \eta_h$ as

$$\mathbf{u}_h(\mathbf{x}) = \sum_{i=1}^{N_F} \mathbf{U}_i \boldsymbol{\varphi}_i^F(\mathbf{x}), \qquad p_h(\mathbf{x}) = \sum_{i=1}^{N_Q} \mathbf{P}_i \phi_i(\mathbf{x}), \qquad \eta_h(\mathbf{x}) = \sum_{i=1}^{N_S} \boldsymbol{\Lambda}_i \varphi_i^S(\mathbf{x}),$$

respectively. By introducing the following matrices:

$$\begin{aligned}
&(\mathbf{A}^F)_{ij} = \mu_F \int_{\Omega^n} \nabla\boldsymbol{\varphi}_i^F : \nabla\boldsymbol{\varphi}_j^F \,\mathrm{d}\mathbf{x}, && (M^F)_{ij} = \rho_F \int_{\Omega^n} \boldsymbol{\varphi}_i^F \cdot \boldsymbol{\varphi}_j^F \,\mathrm{d}\mathbf{x},\\
&(\mathbf{B})_{ij} = -\int_{\Omega^n} \phi_j \,\mathrm{div}\boldsymbol{\varphi}_i \,\mathrm{d}\mathbf{x}, && (\mathbf{T})_{ij} = \rho_F \int_{\Omega^n} [(\mathbf{w}_h^n \cdot \nabla)\boldsymbol{\varphi}_i^F] \cdot \boldsymbol{\varphi}_j^F \,\mathrm{d}\mathbf{x},\\
&(\mathbf{A}^S)_{ij} = \mu_S \int_{\Gamma_0} \frac{\partial\varphi_i^S}{\partial z}\frac{\partial\varphi_j^S}{\partial z} \,\mathrm{d}x_1, && (\mathbf{M}^S)_{ij} = \int_{\Gamma_0} \varphi_i^S \varphi_j^S \mathrm{d}x_1,
\end{aligned}$$

we can rewrite the Galerkin approximation of the fluid sub-problem (4.1)as the following linear system

$$\begin{bmatrix} \frac{1}{\Delta t}\mathbf{M}^F - \mathbf{T} + \mathbf{A}^F & \mathbf{B}^T \\ \mathbf{B} & \mathbf{0} \end{bmatrix} \begin{bmatrix} \mathbf{U} \\ \mathbf{P} \end{bmatrix} = \begin{bmatrix} \frac{1}{\Delta t}\mathbf{M}^F\,\mathbf{U}^n \\ \mathbf{0} \end{bmatrix}.$$

Similarly, the Galerkin solid sub-problem (4.2) can be equivalently rewritten as

$$\left[\left(\frac{\rho_S h_S}{\Delta t^2} + \beta\right)\mathbf{M}^S + \mathbf{A}^S\right]\boldsymbol{\Lambda} = \mathbf{F}^S + 2\frac{\rho_S h_S}{\Delta t^2}\mathbf{M}^S\boldsymbol{\Lambda}^n - \frac{\rho_S h_S}{\Delta t^2}\mathbf{M}^S\boldsymbol{\Lambda}^{n-1},$$

where

$$(\mathbf{F}^S)_j = \int_{\Gamma_0} f_h\,\varphi_j^S \,\mathrm{d}x_1.$$

Similar results yield for the Galerkin approximation of the fluid sub-problem (4.4) and the solid sub-problem (4.5) in the numerical scheme for the iterative solution of the adjoint FSI problem.

## Appendix D. Numerical algorithms

**Algorithm 1:** State FSI problem solver.

**Input:** a tolerance $\tau$ and $\eta_0$
**for** $n = 1, \ldots, N$ **do**
  $j \longrightarrow 1$
  $\eta_0 \longleftarrow \eta^{n-1}$
  **while** $\|\eta_j - \eta_{j-1}\| < \tau$ **do**
    $(\mathbf{u}_j, p_j) \longleftarrow$ fluid sub-problem (4.1)
    $\eta_j \longleftarrow$ structural sub-problem (4.2)
    $\eta_j \longleftarrow \gamma\eta_j + (1-\gamma)\eta_{j-1}$; $j \longleftarrow j+1$
  **end while**
  $(\mathbf{u}^n, p^n, \eta^n) \longleftarrow (\mathbf{u}_j, p_j, \eta_j)$
  $\Omega^{n+1} \longleftarrow \mathcal{A}(\Omega^n)$
**end for**

**Algorithm 2:** Adjoint FSI problem solver.

**Input:** a tolerance $\tau$ and $(\mathbf{u}^n, p^n, \eta^n)\ \forall n = 0, \dots, N$
**for** $n = N-1, \dots, 0$ **do**
  $j \longrightarrow 1$
  $\psi_0 \longleftarrow \psi^{n+1}$
  **while** $\|\psi_j - \psi_{j-1}\| < \tau$ **do**
    $(\mathbf{v}_j, q_j) \longleftarrow$ fluid adjoint sub-problem (4.4)
    $\psi_j \longleftarrow$ structural adjoint sub-problem (4.5)
    $\psi_j = \omega\psi_j + (1-\omega)\psi_{j-1}$; $j \longleftarrow j+1$
  **end while**
  $(\mathbf{v}^n, q^n, \psi^n) \longleftarrow (\mathbf{v}_j, q_j, \psi_j)$
**end for**

**Algorithm 3:** Steepest descent method for shape optimization.

**Input:** reference domain $\Omega^{(0)}$, $J_{new} = J^{(0)}$, tolerance $\tau > 0$
$k \longleftarrow 0$
**while** $|J_{new} - J_{old}| \leq \tau$ **do**
  $J_{old} \longleftarrow J_{new}$
  solve the FSI state problem; evaluate the cost functional $J_{new} = J(\Omega^{(k)})$
  solve the FSI adjoint problem
  evaluate the gradient of the cost functional $\nabla J(\Omega^{(k)})$ according to (3.20) on each design variables
  $\Omega^{(k+1)} \longleftarrow \mathbf{F}(\Omega^{(k)})$ according to the NURBS-FFD map (see Sect. 4.3); $k \longleftarrow k+1$
**end while**

*Acknowledgements.* We are grateful to Prof. Sandro Salsa (Politecnico di Milano) for his valuable insights, to Dr. Luca Dedè (EPFL) for his careful remarks and to Dr. Davide Forti (EPFL) for his useful suggestions. We also acknowledge the anonymous referees for the careful reading of the manuscript and for their many insightful comments.

## References

[1] G. Allaire, Conception Optimale de Structures. Springer Verlag Berlin Heidelberg (2006).
[2] G. Allaire and O. Pantz, Structural optimization with FreeFem++. *Struct. Multidisc. Optim.* **32** (2006) 173–181.
[3] I. Babuška, The finite element method with Lagrange multipliers. *Num. Math.* **20** (1972) 179–192.
[4] S. Badia, F. Nobile and C. Vergara, Fluid-structure partitioned procedures based on Robin transmission conditions. *J. Comput. Phys.* **227** (2008) 7027–7051.
[5] S. Badia, F. Nobile and C. Vergara, Robin-Robin preconditioned Krylov methods for fluid-structure interaction problems. *Comput. Methods Appl. Mech. Engrg.* **198** (2009) 2768–2784.
[6] F. Ballarin, A. Manzoni, G. Rozza and S. Salsa, Shape optimization by free-form deformation: existence results and numerical solution for Stokes flows. *J. Sci. Comput.* **60** (2014) 537–563.
[7] R. Becker and B. Vexler, Optimal control of the convection-diffusion equation using stabilized finite element methods. *Num. Math.* **106** (2007) 349–367.
[8] H.-J. Bungartz and M. Schäfer, Fluid-Structure Interaction. Modelling, Simulation, Optimisation. Vol. 53 of *Lect. Notes Comput. Sci. Eng.* (2006).
[9] P. Causin, J.F. Gerbeau and F. Nobile, Added-mass effect in the design of partitioned algorithms for fluid-structure problems. *Comput. Meth. Appl. Mech. Engrg.* **194** (2005) 4506–4527.
[10] A. Chambolle, B. Desjardins, M.J. Esteban and C. Grandmont, Existence of weak solutions for the unsteady interaction of a viscous fluid with an elastic plate. *J. Math. Fluid Mech.* **7** (2005) 368–404.
[11] P. Crosetto, S. Deparis, G. Fourestey and A. Quarteroni, Parallel algorithms for fluid-structure interaction problems in haemodynamics. *SIAM J. Sci. Comput.* **33** (2011) 1598–1622.
[12] P. Crosetto, P. Reymond, S. Deparis, D. Kontaxakis, N. Stergiopulos and A. Quarteroni, Fluid-structure interaction simulation of aortic blood flow. *Comput. Fluids* **43** (2011) 46–57.
[13] M.C. Delfour and J.P. Zolésio, Shape and Geometries: metrics, analysis, differential calculus and optimization. Society for Industrial and Applied Mathematics (2011).

[14] E.H. Dowell and K.C. Hall, Modeling of fluid-structure interaction. *Annu. Rev. Fluid Mech.* **33** (2001) 445–490.
[15] K. Eppler and H. Harbrecht, Shape optimization for free boundary problems – analysis and numerics. In Constrained Optimization and Optimal Control for Partial Differential Equations. Edited by G. Leugering, S. Engell, A. Griewank, M. Hinze, R. Rannacher, V. Schulz, M. Ulbrich and S. Ulbrich. Springer Basel (2012) 277–288.
[16] L.C. Evans, Partial differential equations. Graduate studies in mathematics. American Mathematical Society (1998).
[17] C. Farhat, M. Lesoinne and P. Le Tallec, Load and motion transfer algorithms for fluid/structure interaction problems with non-matching discrete interfaces: Momentum and energy conservation, optimal discretization and application to aeroelasticity. *Comput. Meth. Appl. Mech. Eng.* **157** (1998) 95–114.
[18] M.A. Fernàndez and J.F. Gerbeau, Algorithms for fluid-structure interaction problems. In Cardiovascular Mathematics. Vol. 1 of *Modeling, Simulation and Applications (MS&A)*. Edited by L. Formaggia, A Quarteroni and A. Veneziani. Springer Verlag Italia, Milano (2009).
[19] M.A. Fernàndez, J.F. Gerbeau and C. Grandmont, A projection semi-implicit scheme for the coupling of an elastic structure with an incompressible fluid. *Int. J. Numer. Methods Eng.* **69** (2007) 794–821.
[20] L. Formaggia and F. Nobile, A stability analysis for the arbitrary Lagrangian Eulerian formulation with finite elements. *East-West J. Numer. Math.* **7** (1999) 105–131.
[21] I. Fumagalli, N. Parolini and M. Verani, Shape optimization for Stokes flow: a reference domain approach. *ESAIM: M2AN* (2015) **49** 921–951.
[22] L. Gerardo-Giorda, F. Nobile and C. Vergara, Analysis and optimization of Robin-Robin partitioned procedures in fluid-structure interaction problems. *SIAM J. Numer. Anal.* **48** (2010) 2091–2116.
[23] M.D. Gunzburger, Perspectives in flow control and optimization. SIAM, Philadelphia (2003).
[24] M.D. Gunzburger, L. Hou and T.P. Svobodny, Optimal control and optimization of viscous, incompressible flows. In Incompressible Computational Fluid Dynamics, edited by M.D. Gunzburger and R.A. Nicolaides. Cambridge University Press (1993) 109–150.
[25] J. Haslinger and R.A.E. Mäkinen, Introduction to Shape Optimization: Theory, Approximation and Computation. SIAM (2003).
[26] C. Heinrich, R. Duvigneau and L. Blanchard, Isogeometric shape optimization in fluid-structure interaction. Rapport de recherche no 7639, INRIA (2011).
[27] M. Hinze, R. Pinnau, M. Ulbrich and S. Ulbrich, Optimization with PDE Constraints. Springer, Netherlands (2009).
[28] K. Ito and K. Kunisch, Lagrange Multiplier Approach to Variational Problems and Applications. *Advances in Design and Control* SIAM (2008).
[29] A. Jameson, Aerodynamic design via control theory. *J. Sci. Comput.* **3** (1988) 233–260.
[30] A. Jameson, Optimum aerodynamic design using cfd and control theory. In *Proc. of the 12th AIAA Computational Fluid Dynamics Conference*. AIAA Paper 95–1729. (1995) 926–949.
[31] H.J. Lamousin and W.N. Waggenspack, NURBS-based free-form deformations. *IEEE Comput. Graph. Appl.* **14** (1994).
[32] T. Lassila, A. Manzoni, A. Quarteroni and G. Rozza, Boundary control and shape optimization for the robust design of bypass anastomoses under uncertainty. *ESAIM: M2AN* **47** (2013) 1107–1131.
[33] T. Lassila, A. Manzoni, A. Quarteroni and G. Rozza, A reduced computational and geometrical framework for inverse problems in haemodynamics. *Int. J. Numer. Methods Biomed. Engng.* **29** (2013) 741–776.
[34] P. Le Tallec and J. Mouro, Fluid structure interaction with large structural displacements. *Comput. Meth. Appl. Mech. Engrg.* **190** (2001) 3039–3067.
[35] Y. Maday, Analysis of coupled models for fluid-structure interaction of internal flows. In Cardiovascular Mathematics, edited by L. Formaggia, A Quarteroni and A. Veneziani. Vol. 1 of Modeling, Simulation and Applications (MS&A). Springer Verlag Italia, Milano (2009).
[36] A. Manzoni, A. Quarteroni and G. Rozza, Shape optimization of cardiovascular geometries by reduced basis methods and free-form deformation techniques. *Int. J. Numer. Methods Fluids* **70** (2012) 646–670.
[37] B. Mohammadi and O. Pironneau, Applied shape optimization for fluids. Oxford University Press (2009).
[38] M. Moubachir and J.P. Zolésio, Moving Shape Analysis and Control. Applications to Fluid Structure Interactions. Chapman and Hall (2006).
[39] B. Muha and S. Canić, Existence of a weak solution to a nonlinear fluid-structure interaction problem modeling the flow of an incompressible, viscous fluid in a cylinder with deformable walls. *Arch. Rat. Mech. Anal.* **207** (2013) 919–968.
[40] F. Negri, A. Manzoni and G. Rozza, Reduced basis approximation of parametrized optimal flow control problems for the Stokes equations. *Comput. Math. Appl.* **69** (2015) 319–336.
[41] F. Nobile and C. Vergara, An effective fluid-structure interaction formulation for vascular dynamics by generalised robin conditions. *SIAM J. Sci. Comput.* **30** (2008) 731–763.
[42] W.F. Noh, A time-dependent two-space-dimensional coupled Eulerian-Lagrangian code. *Methods in Comput. Phys.* **3** (1964) 117–179.
[43] N. Parolini and A. Quarteroni, Mathematical models and numerical simulations for the America's Cup. *Comput. Meth. Appl. Mech. Engrg.* **194** ( 2005) 1001–1026.
[44] L. Piegl and W. Tiller, The NURBS Book. Springer (1997).
[45] A. Quarteroni, G. Rozza, L. Dedè and A. Quaini, Numerical approximation of a control problem for advection-diffusion processes. In *System Modeling and Optimization: Proceedings of the 22nd IFIP TC7 Conference*, edited by F. Ceragioli, A. Dontchev, H. Futura, K. Marti and L. Pandolfi. Springer US (2006) 261–273.

[46] A. Sacharow, S. Odendahl, A. Peuker, D. Biermann, T. Surmann and A. Zabel, Iterative, simulation-based shape modification by free-form deformation of the nc programs. *Adv. Engine. Soft.* **56** (2013) 63–71.

[47] R.F. Sarraga, Modifying cad/cam surfaces according to displacements prescribed at a finite set of points. *Comput. Aided Design* **36** (2004) 343–349.

[48] S. Schäfer, D.C. Sternel, G. Becker and P. Pironkov, Efficient numerical simulation and optimization of fluid-structure interaction. Fluid Structure Interaction II. In Vol. 73 of Lect. *Notes Comput. Sci. Eng.* (2010) 131–158.

[49] T.W. Sederberg and S.R. Parry, Free-form deformation of solid geometric models. *Comput. Graph.* **20** (1986) 151–160.

[50] J. Sokolowski and J.P. Zolésio, Introduction to Shape Optimization: Shape Sensitivity Analysis. Springer Verlag Berlin Heidelberg (1992).